LA-10012-SR
Status Report

UC-33a
Issued: June 1984

LA--10012-SR

DE84 015978

General-Purpose Heat Source Development: Safety Test Program

Postimpact Evaluation, Design Iteration Test 2

F. W. Schonfeld
T. G. George

Los Alamos National Laboratory
Los Alamos, New Mexico 87545

GENERAL-PURPOSE HEAT SOURCE DEVELOPMENT: SAFETY TEST PROGRAM

Postimpact Evaluation, Design Iteration Test 2

by

F. W. Schonfeld and T. G. George

ABSTRACT

The General-Purpose Heat Source (GPHS) provides power for space missions by transmitting the heat of $^{238}PuO_2$ decay to thermoelectric elements. Because of the inevitable return of certain missions, the heat source must be designed and constructed to survive both re-entry and Earth impact. The Design Iteration Test (DIT) series is part of an ongoing test program. In the first Design Iteration Test (DIT-1), a full GPHS module containing four iridium-alloy capsules loaded with $^{238}PuO_2$ was impacted at 57 m/s and 930°C. All four capsules survived and none was breached. The capsules used in DIT-1 were loaded and welded at Los Alamos. The second Design Iteration Test (DIT-2) also used a full GPHS module and was impacted at 58 m/s and 930°C. The four iridium-alloy capsules used in this test were loaded and welded at the Savannah River Plant (SRP). Postimpact examination revealed that two capsules had survived and two capsules had breached; a small quantity (≈50 μg) of $^{238}PuO_2$ was released from the breached capsules. Internal cracking similar to that observed in the DIT-1 capsules was evident in all four of the DIT-2 capsules. Postimpact analyses of the units are described with emphasis on weld structure and performance.

I. INTRODUCTION

The General-Purpose Heat Source (GPHS) will provide power for a number of space missions. The first two uses will be the 1986 Galileo and International Solar-Polar Missions. The GPHS unit uses the heat of $^{238}PuO_2$ alpha decay to generate power by means of a thermoelectric array. In addition to the inevitable return of near-Earth missions, the probability of a launch failure can never be zero. Therefore, the GPHS module must be designed and constructed to survive both re-entry and Earth impact. The test results described in this report are a portion of the ongoing impact program and will provide necessary design information.

The first Design Iteration Test (DIT-1) was carried out at a velocity of 57 m/s and 930°C (as measured on the outer surface of the iridium-alloy capsules).[1] The test unit was a full GPHS module that contained two graphite impact shells (GISs); each GIS contained two heat source capsules filled with $^{238}PuO_2$. All of the capsules were loaded and welded at Los Alamos. The four pellets provided a total thermal power of 250 W. The major

concern in DIT-1 was the quality and survivability of the welds. All of the capsules survived impact, and none of the capsules breached. Postimpact analysis revealed that the welds were of consistently good quality and behaved no differently than the surrounding material. Intergranular cracking was observed on the welds and capsule walls; some cracks traversed more than 70% of the wall thickness.

The second Design Iteration Test (DIT-2) was carried out at a velocity of 58 m/s and 930°C. The test unit was a full GPHS module. The four DIT-2 capsules were fueled and welded at the Savannah River Plant (SRP). As in DIT-1, DIT-2 was concerned primarily with the quality and survivability of the welds. This report, therefore, emphasizes the weld structures and performance.

II. PRETEST DATA

A. Fuel Pellets and Iridium-Alloy Cups

The iridium-alloy cups and fuel pellets used in the individual heat source assemblies are identified in Table I; data describing the fuel pellets are in Table II. The iridium cups and fuel pellets used in DIT-2 were similar to those used in DIT-1. The SRP produced the fuel pellets; Oak Ridge National Laboratory (ORNL) provided the iridium-alloy blanks; the Mound Facility (MF) fabricated the iridium cups; ORNL produced the graphite insulation [carbon-bonded carbon filament (CBCF)]; and Los Alamos machined the aeroshell and impact shells from Fineweave-Pierced Fabric* (FWPF) graphite. DIT-1 and DIT-2 differ in two ways: (1) The fuel clads used in DIT-2 were loaded and welded at SRP, whereas the fuel clads used in DIT-1 were loaded and welded at Los Alamos. (2) The weld overlaps of the DIT-1 capsules were positioned in the GISs so as to minimize deformation on impact (weld overlaps pointed toward the trailing face of the aeroshell), whereas the DIT-2 capsules were loaded in the GISs with the weld overlaps near or against the impact face. (Note that there is no locking mechanism in the standard graphite assembly, and both the fuel clads and GISs are free to rotate during handling.) Impact temperatures (930°C) and velocities (57 m/s) were reproduced within engineering tolerances. The postimpact procedures applied in DIT-2 were in general the same as those used in DIT-1; however, they did differ in detail as judged appropriate.

*Fineweave-Pierced Fabric 3-D carbon/carbon composite, a product of AVCO Systems Division, 201 Lowell St., Wilmington, MA 01887.

TABLE I. Encapsulation Details for DIT-2 Fueled Clads.

	Iridium Cup		
Capsule No.	Vent	Weld Shield	Fuel Pellet
SR-105	MER1-2	N505-6	SR-105
SR-106	N504-5	MERR3-3	SR-106
SR-107	LR300-2	MR432-2	SR-107
SR-110	N515-3	NR516-6	SR-110

TABLE II. Data for Sintered DIT-2 Fuel Pellets.

Identification	Diameter (mm)	Length (mm)	Weight (g)
SR-105	27.61	27.21	149.0
SR-106	27.58	27.69	148.8
SR-107	27.65	27.72	148.5
SR-110	27.72	27.77	149.2

B. Weld Examinations

The four fuel pellets used in DIT-2 were identified as SR-105, SR-106, SR-107, and SR-110. To avoid unnecessary complication, these fuel labels are used throughout this report to identify the fuel/clad sets.

Each of the four capsules was macroscopically examined for weld defects. The macrostructures of the weld overlaps are shown in Fig. 1. All overlaps were uniform and contained no obvious defects: the welds appeared to be of good quality. In capsules SR-105, SR-106, and SR-110, there was no bulging at the weld overlap, and there appeared to be good wall alignment over the entire weld length. Capsule SR-107 was slightly bulged at the weld overlap (≈0.003 in.).

III. TEST PROCEDURE

After macroscopic examination the four capsules were loaded into GISs. The loaded GISs were then heat treated at 1300°C for 100 h, primarily for stress relief of the weld. Following heat treatment the GISs were loaded into the aeroshell as shown in Fig. 2. Note that the closure-weld-overlap areas were oriented toward the impact face.

The test conditions were 930°C and 58 m/s. After the test, a catch tube containing the impacted module was transferred to Wing 2 of the CMR Building (at Los Alamos) and opened in a hood.

IV. POSTIMPACT EXAMINATION

Experience with DIT-1 speeded postimpact disassembly. The catch tube was opened without difficulty; no contamination was found on the samples or lid. The inner nickel can (a radiation shield assembly) was extracted with tongs, and the can/aeroshell/heat source assembly was placed on a bed of solid CO_2. The CO_2 cooled the assembly rapidly, and in a few seconds the temperature had dropped far enough to eliminate the possibility of graphite combustion. The aeroshell was fractured but not as severely as the aeroshell used in DIT-1. Although the damaged aeroshell (Fig. 3) was deformed in a uniform manner, when the GISs were extracted, GIS-2 was noticeably more broken than was GIS-1. GIS-1 and GIS-2 are shown in Figs. 4 and 5.

The fuel capsules were extracted from the GIS, photographed, and measured. Capsule dimensions and the calculated gross strains are listed in Tables III and IV. Capsules SR-107 and SR-110 exhibited the same deformation mode observed in the DIT-1 capsules: the capsules were flattened on the impact side and had protrusions at a position corresponding to the unsupported side of the GIS. The capsules removed from GIS-2 were more symmetrical. Side and end views of all four capsules may be seen in Fig. 6. Although the cracks are barely visible in Fig. 6, SR-107 and SR-110 were breached on the leading side of the radius on the vent ends.

V. CAPSULE OPENING AND CAPSULE FUEL SAMPLING

A. Cutting Procedure

Because the four impacted capsules in DIT-2 were similar to each other and to the capsules from DIT-1, the same opening procedure was used. An abrasive slitting wheel was used to make a small circumferential cut 6-8 mm above the weld (vent side) on each capsule. Contact between the abrasive wheel and the fuel pellet was minimized by minimizing the actual breakthrough of the capsule wall. The remaining iridium-alloy wall on

TABLE III. Dimensions (in inches) of DIT-2 Fuel Clads.

	Diameter			Length	
Capsule	Vent Cup	Blind Cup	Weld	Capsule	Diagonal
SR-105					
Before impact	1.173	1.174	1.180	1.186	1.4765
After (min)	1.107	1.130	1.143	1.181	1.50
(max)	1.240	1.233	1.240	1.227	1.42
SR-106					
Before impact	1.180	1.175	1.180	1.188	1.480
After (min)	1.110	1.115	1.117	1.200	1.418
(max)	1.217	1.235	1.255	1.228	1.490
SR-107					
Before impact	1.176	1.176	1.180	1.186	1.478
After (min)	1.118	1.105	1.130	1.185	1.446
(max)	1.230	1.232	1.267	1.250	1.514
SR-110					
Before impact	1.175	1.175	1.181	1.185	1.476
After (min)	1.100	1.089	1.112	1.210	1.425
(max)	1.250	1.250	1.285	1.264	1.514

TABLE IV. Gross Strains in DIT-2.

	SR-105 (%)	SR-106 (%)	SR-107 (%)	SR-110 (%)
Height				
Edge	3.5	3.4	5.4	6.7
Center	0.4	1.0	0.2	2.1
Diametral				
Top	5.7	3.2	4.6	6.4
Weld	5.1	6.3	7.4	8.8
Bottom	5.0	4.0	4.8	6.4
Top	-5.7	-5.9	-4.9	-6.4
Weld	-3.2	-5.4	-4.2	-5.8
Bottom	-3.8	-5.1	-6.0	-7.3
Diagonal	1.6	0.7	1.5	2.6
	0.9	0.5	0.4	0.6
	-3.8	-4.2	-5.1	-3.5
	-2.1	-1.2	-2.2	-1.8

SR-105, SR-106, and SR-107 was pried open with a small screwdriver; the clads were defueled immediately after opening. SR-110 was transferred to the glove-box train used for fines analysis before opening (under H_2O to avoid the loss of any small particles).

B. Macroscopic Examination

The opened capsules were examined with a hand-held magnifier. No external cracks were visible in the closure weld area on any capsule. SR-107 and SR-110, however, were breached in the radiused portions of the vent cups. The breaching cracks seemed to initiate on the outer surfaces and propagate inward. The cracking apparently resulted from two successive bends: the first (inward) early in the impact event and the second (outward) as the crushed fuel exerted an internal pressure. In both cases the fracture was narrow at the interior surface (0.025 to 0.050 mm) and would be expected to release only a small quantity of fuel. Subsequent analysis revealed that GIS-1 contained 0.03 mg of fuel and GIS-2 contained 0.022 mg. Several fine cracks were observed in the welds and walls of all four capsules. All cracked areas were removed for metallographic examination.

C. Weld and Wall Sampling

A face-on weld sample was obtained from each capsule in accordance with SRP procedure DPSOL 235-F PuFF-3129M.[2] Welds in the overlap and single-pass regions from each capsule were sampled also. The weld samples included enough wall to establish grain size, other microstructural features, and hardness of the weld-shield cup. Similarly, the vent cup sections included enough wall to establish grain size and reveal other microstructural features.

Samples of the two cups making up each capsule were submitted for spectrographic and Auger electron spectrographic analyses. These samples were cut from the cup walls at about midheight.

D. Fuel Sampling

We selected two fragments, each weighing $\approx$1 g, from the fuel from each capsule (SR-105, -106, and -107) and examined the fragments by ceramography: one fragment was removed from the outer edge of the fuel pellet, and one fragment was removed from the pellet center. Two additional 1-g fragments were obtained for chemical

TABLE V. Sieve Analysis of the Fuel from Capsule SR-110.

Particle Size (m)	Weight Fraction	Accumulated Weight Fraction
+6000	0.4620	0.4620
+2000	0.3463	0.8083
+ 841	0.1269	0.8352
+ 420	0.0304	0.9656
+ 177	0.0125	0.9781
+ 125	0.0027	0.9808
+ 74	0.0042	0.9850
+ 45	0.0031	0.9880
+ 30	0.0043	0.9922
+ 20	0.0024	0.9947
+ 10	0.0044	0.9991
- 10	0.0009	1.0000
$\leq$ 4	0.0001	

analysis: one fragment for spectroscopic examination and one for a wet-chemistry phosphorus determination. The fuel in capsule SR-110 was not sampled until a particle-size analysis had been completed; results of the particle-size analysis are presented in Table V. When the fuel samples had been repackaged for transfer, each lot was radioanalyzed to approximate the phosphorus content.

VI. METALLOGRAPHIC EXAMINATION

A. Cracks in the Iridium/0.3 wt% W Alloy

Because capsules SR-107 and SR-110 had breached and the welds and walls of all four capsules had cracked, the weld samples required by SRP procedure DPSOL 235-F-PuFF-3129M were obtained after the cracked samples had been examined.

In capsule SR-105, a cluster of three cracks was observed in the weld bead. These cracks, shown in Fig. 7, were intergranular in nature (between columnar grains) and did not appear to extend into the capsule wall. Subsequent metallographic examination of a section parallel to the weld revealed that the cracks did extend into the capsule wall and that the extent of their penetration was approximately 50% (Fig. 8). The geometric relationships between the cracks, the weld, and the capsule cross section are illustrated in Fig. 9; also indicated are the locations where SRP nondestructive-testing personnel found magnitude 4 or greater weld cracks.[3] (Figure 9 uses the weld termini as base points for measurement.)

Capsule SR-106 contained more weld cracks than any other DIT-2 capsule. Inspection revealed three crack families (Fig. 10) that apparently were generated by bending. Figure 11 describes the microstructures of these cracks and the associated alloy; Fig. 9 shows the crack locations.

The interior surface of capsule SR-107 had numerous cracks where reverse bending occurred. This area contained at least 9 cracks in the weld bead and 12 cracks in the capsule wall (Figs. 12 and 13). The locations of these cracks are shown in Fig. 9. Some cracks were limited to the weld bead, whereas others were restricted to the base metal; several cracks traversed both the weld and capsule wall. The appearance of these cracks suggests that susceptibility to cracking during bending is slightly greater in the weld bead than in the unaltered wall. This relatively small difference would appear to reflect slight differences in grain morphology rather than a change in basic character.

Figure 14 shows the breach in the vent-end radius of capsule SR-107. A two-stage bending action seems to have produced the crack; it appears that the capsule bent inward during the first stage of impact, then outward as the bulk density of the fuel and internal volume of the capsule decreased. Microhardness testing revealed that the alloy adjacent to the crack was significantly harder than was material that had not been deformed. The wall section adjacent to the crack had an average Vickers hardness greater than 400; the Vickers hardness of undeformed wall sections averaged 330. (The results of Vickers microhardness tests conducted on selected sections of all four iridium-alloy capsules are presented in Table VI.) The crack location was apparently influenced

TABLE VI. Postimpact Hardness of Iridium-Alloy Capsules Used in DIT-2.

	SR-105		SR-106		SR-107		SR-110	
	95% CL[a]	Range	95% CL	Range	95% CL	Range	95% CL	Range
V cup[b]								
Undeformed	337 ± 14	296-382	327 ± 19	289-369	360 ± 8	347-375	316 ± 9	289-333
Deformed	399 ± 15	376-418	386 ± 8	375-396	413 ± 16	391-432	410 ± 27	370-441
WS cup[c]								
Undeformed	319 ± 7	305-342	344 ± 11	325-376	316 ± 4	303-328	316 ± 16	296-340
Deformed	388 ± 13	396-404	406 ± 24	360-432	431 ± 25	399-463	370 ± 12	349-395
Weld								
Single Pass	348 ± 13	304-376	350 ± 20	280-369	325 ± 8	309-340	310 ± 11	291-324
Overlap	---	---	302 ± 10	289-316	---	---	---	---

[a]CL = confidence level.
[b]The cup containing the vent.
[c]The cup containing the weld shield.

by the proximity of the welded vent-assembly, which increased the stiffness of the capsule and tended to localize deformation. Also, bending in the center of the GIS may make the vent ends (which were pointed toward the center of the GIS) recipients of a higher impulse.

Capsule SR-110 deformation mirrored that of SR-107, including the crack which breached the wall in the radiused portion of the vent end. However, note that the crack in SR-110 was slightly higher and closer to the vent. Internal cracking of the weld bead in SR-110 was not nearly as extensive as that found in capsule SR-107. We observed only one set of cracks in the SR-110 weld bead (Fig. 15). Figure 9 shows the location of these cracks relative to the weld submergence and end. The breaching crack is shown in Fig. 10.

B. Weld Metallography

The equatorial weld of capsule SR-105 was sampled in cross sections taken from the single-pass, overlap, and face-on weld areas in accordance with SRP procedure DPSOL 235-F-PuFF. The microstructures of the three samples (Figs. 17a-c) are typical with no observed defects.

Weld samples were taken from capsule SR-106 to show the single-pass, overlap, and face-on weld structures. The microstructure of the single-pass sample is shown in Fig. 18; the structure is similar to the single-pass sample removed from capsule SR-105. The overlap sample from SR-106 contained a centerline crack that penetrated over 30% of the wall thickness (Fig. 19). Although the capsule was severely deformed on impact and brittle grain-boundary cracks look much the same regardless of origin, the centerline crack in SR-106 appears to be a weld crack. (The crack runs parallel to the weld direction; cracks resulting from impact usually run perpendicular to the weld.) The face-on section of the single-pass weld, shown in Fig. 20, revealed typical structure and contained no observable defects.

The single-pass weld section of capsule SR-107, shown in Fig. 21, appeared to be sound and contained no unusual microstructural features. The overlap cross section was quite porous (Fig. 22a). This porosity was largely confined to the grain boundaries of the remnant first-pass weld metal (Fig. 22b). Figure 22c verifies this observation within the central portion of the weld bead; Fig. 22d shows that the same phenomenon is present at the root of the weld bead.

Figures 22c and d clearly indicate that gas evolution can take place at grain boundaries in the weld metal when it is reheated to temperatures approaching the melting point. Figure 23 (SR-105) demonstrates that this type of porosity can be produced in wrought as well as cast (weld bead) iridium alloy. The section shown in Fig. 23 was cut parallel to the weld direction and slightly above the centerline and includes both unmelted wall and weld bead. Reverse bending on impact seems to have produced the crack that originated on the inside surface, and grain-boundary porosity obviously contributed to the failure. Whether the gas evolution that causes grain-boundary porosity is independent of or part of the "hot short" weld cracking problem, which we observed previously, is unclear; however, some degree of interaction is likely.

The face-on section of the single-pass weld in capsule SR-107, shown in Fig. 24, revealed typical structure and contained no observable defects.

The three weld sections (single-pass, overlap, and face-on) removed from capsule SR-110 contained no significant defects. The single-pass sample was sound and had a typical microstructure (Fig. 25). The weld bead in the overlap section contained a few small pores (Fig. 26a); otherwise, microstructure was typical (Fig. 26b). Figure 27 illustrates typical face-on weld structure.

C. Vent Metallography

The four vent structures were carefully examined to determine if the pretest heat treatment (100 h at 1300°C) had caused the transport of any fuel components and to further define the mechanical response of the vent assembly. No mechanical defects were observed in any of the vent sections. All of the frits were uniform and properly aligned. No significant amounts of fuel impurities were detected in the vent cross sections. All vents, shown in Figs. 28 through 31, survived the test without significant damage. The SR-106 and SR-107 vents exhibited a small amount of plastic strain, and the SR-110 vent weld had a small crack. However, these defects are minor, and the overall response of the four vents is satisfactory.

D. Iridium Cup Wall Microstructure

One sample was obtained from the wall of each capsule and prepared for metallographic examination.

Before loading, the iridium-alloy capsules had been heated (20 h at 1500°C) to produce a grain size approximating that present after six months of service (13-14 grains/0.635-mm wall thickness, as predicted by ORNL[4]); a second preimpact heat treatment relieved welding stresses (100 h at 1300°C). Because the heat sources were never exposed to temperatures higher than those used in preimpact heat treatments, we expected pre- and postimpact grain size and microstructure to be the same (with the exception of areas that experienced substantial deformation). Microscopic examination revealed that the DIT-2 capsules had grain sizes ranging from 18 to 26 grains/0.635-mm thickness. Figures 32 through 35 show the grain size and microstructure of each sample; Table VII lists the measured grains/thickness (normalized to a 0.635-mm wall thickness). All microstructures were typical, and the behavior of these capsules should be considered as representative of the "average" impact response.

VII. FUEL CERAMOGRAPHY

All DIT-2 fuel pellets fractured in a similar manner; apparently, each fuel pellet responded to the impact stresses by fracturing in a completely brittle mode. Figures 36 and 37 show the general patterns of fuel breakup. Although pellet SR-106 contained large cracks before testing [identified by Los Alamos radiographic inspection (Fig. 36)] and capsules SR-107 and SR-110 experienced larger total deformations than SR-105 or SR-106, the fuel fracture mechanism was apparently the same in all four pellets.

Ceramographic samples from each pellet provided structural pellet-to-pellet and edge-to-center comparisons. Photomicrographs of fuel pellet microstructures (Figs. 38 through 45) reveal that some degree of microstructural variation exists between pellets and from point to point within a given pellet. These slight variations apparently had little effect on the overall pellet performance, as the mechanical responses of all four pellets were essentially the same.

TABLE VII. Grain Sizes of DIT-2 Capsules [Grains/wall thickness (G/T) normalized to 0.025 in.]

	Vent Cup		Weld-Shield Cup	
Capsule	Ident. No.	G/T	Ident. No.	G/T
SR-105	MER 1-2	26	N 505-6	21
SR-106	N 504-5	18	MERR 3-3	25
SR-107	LR 300-2	20	MR 432-2	20
SR-110	N 515-3	21	NR 516-6	21

VIII. CHEMICAL ANALYSES

A. Iridium-Alloy Chemistry

Samples from the walls of the eight iridium-alloy cups used in DIT-2 were removed for chemical analysis. The samples were submitted for spectrographic and Auger electron spectroscopic examinations: the spectrographic analysis determined the bulk composition of each sample, and Auger electron spectroscopy determined the distribution of various elements on a fresh fracture surface. Results of the analyses are listed in Tables VIII and IX.

The spectrographic analyses in Table VIII indicate that the iridium alloy was of good overall purity and that there was little chemical variation from cup to cup.

The Auger data, given in Table IX, suggest that thorium segregated to the grain boundaries of both cast (weld bead) and recrystallized alloy. Relative grain orientations, cooling rates, and other less obvious factors probably influenced the degree of thorium concentration, which varied from sample to sample. Also, elements such as sulfur, phosphorus, and silicon may have been present in the grain boundaries. Because carbon and oxygen are present in residual gases contained within the Auger vacuum chamber, the Auger peaks for these elements are generally ignored. The possibility exists, however, that the carbon and oxygen peaks observed in these analyses had a real component; carbon and oxygen may have been present in the iridium grain boundaries.

B. Fuel Chemistry

Samples for chemical analysis were removed from each of the four fuel pellets used in DIT-2. The results of spectrographic surveys, as well as the results of wet and radioanalyses for phosphorus, are presented in Table X. These results indicate that the fuel pellets were chemically similar to one another and to the fuel pellets used in DIT-1. The amounts of magnesium, silicon, calcium, titanium, and tantalum impurities did vary from pellet to pellet, but the overall effect of these impurities is unclear.

TABLE VIII. Spectrographic Analyses[a] of GPHS Clads Used in DIT-2.

	SR-105		SR-106		SR-107		SR-110	
	1 (MER-2)	2 (N-505-6)	3 (N 504-5)	4 (MERR 3-3)	5 (LR 300-2)	6 (MR-432-2)	7 (N 515-3)	8 (NR 576-6)
Element	V cup	WS cup	V cup	WS cup	V cup	WS cup	V cup	WS cup
Li	<100	<DL	<DL	<DL	<DL	<DL	<DL	<DL
Be	<3	<DL	<DL	<DL	<DL	<DL	<DL	<DL
B	<10	<DL	<DL	<DL	<DL	<DL	<DL	<DL
Na	<300	<DL	<DL	<DL	<DL	<DL	<DL	<DL
Mg	25	20	15	3	3	3	15	15
Al	40	50	40	40	40	40	70	50
Si	20	20	20	10	10	10	20	20
P	<300	<DL	<DL	<DL	<DL	<DL	<DL	<DL
K	<3000	<DL	<DL	<DL	<DL	<DL	<DL	<DL
Ca	3	3	<DL	<DL	<DL	<DL	<DL	<DL
Ti	<30	<DL	<DL	<DL	<DL	<DL	<DL	<DL
V	<30	<DL	<DL	<DL	<DL	<DL	<DL	<DL
Cr	<10	<10	<DL	<DL	<DL	<DL	10	10
Mn	<10	<DL	<DL	<DL	<DL	<DL	<DL	<DL
Fe	40	20	20	30	30	30	100	80
Co	<10	<DL	<DL	<DL	<DL	<DL	<DL	<DL
Ni	20	10	<10	20	20	20	50	40
Cu	20	15	5	15	15	15	20	15
Zn	<50	<DL	<DL	<DL	<DL	<DL	<DL	<DL
Ga	<30	<DL	<DL	<DL	<DL	<DL	<DL	<DL
Ge	<30	<DL	<DL	<DL	<DL	<DL	<DL	<DL
Sr	<3	<DL	<DL	<DL	<DL	<DL	<DL	<DL
Zr	<300	<DL	<DL	<DL	<DL	<DL	<DL	<DL
Nb	<300	<DL	<DL	<DL	<DL	<DL	<DL	<DL
Mo	<300	<DL	<DL	<DL	<DL	<DL	<DL	<DL
Ru	<30	<DL	<DL	<DL	<DL	<DL	<DL	<DL
Rh	<30	<DL	<DL	<DL	<DL	<DL	<DL	<DL
Pd	<20	<DL	<DL	<DL	<DL	<DL	<DL	<DL
Ag	<10	<DL	<DL	<DL	<DL	<DL	<DL	<DL
Cd	<100	<DL	<DL	<DL	<DL	<DL	<DL	<DL
In	<30	<DL	<DL	<DL	<DL	<DL	<DL	<DL
Sn	<50	<DL	<DL	<DL	<DL	<DL	<DL	<DL
Sb	<300	<DL	<DL	<DL	<DL	<DL	<DL	<DL
Ba	<3	<DL	<DL	<DL	<DL	<DL	<DL	<DL
Hf	<300	<DL	<DL	<DL	<DL	<DL	<DL	<DL
Ta	<1000	<DL	<DL	<DL	<DL	<DL	<DL	<DL
W	0.1-1%	0.1-1%	0.1-1%	0.1-1%	0.1-1%	0.1-1%	0.1-1%	0.1-1%
Pt	<30	<DL	<DL	<DL	<DL	<DL	<DL	<DL
Au	<10	<DL	<DL	<DL	<DL	<DL	<DL	<DL
Tl	<30	<DL	<DL	<DL	<DL	<DL	<DL	<DL
Pb	<50	<DL	<DL	<DL	<DL	<DL	<DL	<DL
Bi	<30	<DL	<DL	<DL	<DL	<DL	<DL	<DL

[a]Result preceded by < symbol represents limit of detection. To increase clarity, detection limits are indicated in column 1, column 2 (Ca) and (Cr), and column 3 (Ni); <DL means less than detection limit.

TABLE IX. Auger Intensity Ratio. from Wall Samples of GPHS Used in DIT-2.

	Th_{65}/Ir_{229}			Th_{65}/Ir_{542}			Si_{92}/Ir_{229}			P_{120}/Ir_{229}			S_{150}/Ir_{229}			C_{270}/Ir_{229}			O_{510}/Ir_{229}		
Capsule	in.	cen.	out.	in.	cen.	out.	in.	cen.	out.	in.	cen.	out.	in.	cen.	out.	in.	cen.	out.	in.	cen.	out.
Sr-105																					
V cup (1)	0.078	0.069	0.064	0.580	0.500	0.444										0.420	0.448	0.478			0.622
(2)		0.075			0.509												0.237				
WS cup (1)	0.059	0.053	0.069	0.407	0.412	0.439			0.018						0.070	0.833	0.708	1.149	0.806	0.888	0.877
(2)		0.057			0.440												0.510			0.820	
sputtered			0.093			0.020												0.570			
SR-106																					
V cup (1)	0.018	0.046	0.059	0.135	0.381	0.429															
(2)		0.044			0.347																
WS cup (1)	0.074	0.090	0.068	0.483	0.652	0.469										0.367	0.717	0.837	0.475	0.435	0.480
(2)		0.077			0.566												0.462			0.453	
Sr-107																					
V cup (1)	0.048	0.008	0.062	0.346	0.059	0.418								0.025	0.155	0.385	0.490	0.755	0.664	0.363	0.964
(2)		0.005			0.039												0.481			0.433	
sputtered			Tr			Tr								0.019			0.606				
WS cup (1)	0.053	0.052	0.057	0.364	0.357	0.408						0.097	0.109	0.119	0.039	0.491	0.536	0.602	0.782	0.952	0.72d
(2)		0.072			0.533									0.076			0.438			0.971	
sputtered	Tr			Tr																	
SR-110																0.505					
V cup (1)	0.047	0.048	0.063	0.359	0.355	0.480						0.100		0.027		0.576	0.518	0.350	0.755	0.800	0.800
(2)		0.057			0.418												0.764			0.709	
WS cup (1)	0.072	0.073	0.051	0.528	0.537	0.308			0.308					0.031	0.307		0.367	0.539			0.862
(2)		0.063			0.467			0.168			0.112							0.206		0.299	
sputtered	Tr					Tr												0.562			

TABLE X. Chemical Analyses.
Spectrographic Analyses of DIT-2 Fuel

Element	SR-105	SR-106	SR-107	SR-110
Li	1	1	2	2
Be	<1	<1	<1	<1
B	4	3	3	1
Na	5	2	7	2
Mg	100	100	100	20
Al	20	8	30	45
Si	230	180	240	200
K	<5	<5	<5	<5
Ca	250	100	300	150
Ti	150	100	100	60
V	<3	<3	<3	<3
Cr	40	40	30	80
Mn	10	7	8	4
Fe	340	250	300	410
Co	<3	<3	<3	<3
Ni	20	20	20	9
Cu	<1	<1	<1	<1
Zn	8	8	8	<5
Rb	<10	<10	<10	<10
Sr	<5	<5	<5	<5
Y	<25	<25	<25	<25
Zr	<100	<100	<100	<100
Nb	<10	<10	<10	<10
Mo	5	5	4	<3
Ag	10	10	30	5
Cd	<10	<10	<10	<10
Sn	<5	<5	<5	<5
Ba	7	<2	2	<2
La	<25	<25	<25	<25
Hf	<25	<25	<25	<25
Ta	1000	1000	500	100
W	<10	<10	<10	<10
Re	<25	<25	<25	<25
Pb	15	<5	<5	<5
Bi	<1	<1	<1	<1

Results of Radioassay and Wet Analysis for Phosphorus

Element	SR-105	SR-106	SR-107	SR-110
P radio	<20	<20	<20	<20
P wet	25	30	40	25

Their presence would not be expected to affect the impact response; however, the presence of any impurity can affect the kinetics that control impurity transport and vent clogging. The chromium, iron, and nickel values recorded in the spectrographic analyses may reflect contamination from contact with stainless steel tools and enclosures during pellet fabrication and postimpact examination. The amount of phosphorus detected in each pellet was generally the same and was consistent with the phosphorus impurities observed in the DIT-1 fuel pellets.

IX. LOCAL STRAINS

Postimpact examination of the four DIT-2 capsules revealed that capsules SR-107 and SR-110 had been breached. The breaching cracks occurred on the radiused portions of the vent ends and were apparently produced by reverse bending. When the four capsules were opened and defueled, numerous cracks were observed on the interior surfaces of areas that experienced substantial deformation. These cracks were within or adjacent to the weld beads. Figure 12 shows a typical crack pattern from SR-107. The presence of these cracks and the fact that two capsules breached and released a small quantity of fuel indicate that the operable safety margin in this test was zero. Note that areas of appreciable local deformation where failure did not occur were observed in the walls of all four capsules. The maximum local strains observed in the DIT-2 capsules, as measured from enlarged macrographs, are listed in Table XI.

The corner (end-radius) strains in all capsules were significantly larger than the side-wall strains. Although the end radius in two capsules breached, the corners deformed appreciably before failure. The side walls in all capsules cracked at relatively low total strains. This observation supports previous indications that the strain state is at least as important as strain magnitude.

The GIS seems to have deflected at its center during side-on impact (being supported only on the ends), which allowed the FWPF partitions and vent ends of the fuel capsules to contact the aeroshell wall earlier than the remainder of the GIS. Fuel breakup, relative stiffness of the welded vent assembly, and mechanical interaction with the leading edges of the FWPF end plugs and partitions influenced capsule deformation. Substantial deformation apparently occurred at the corner of each capsule before the bulk density of the fuel and internal

TABLE XI. Maximum Local Strains in DIT-2 Capsules.

	SR-105 (%)	SR-106 (%)	SR-107 (%)	SR-110 (%)
Circumference	6.4	7.9	7.9	6.0
End (radius) (vent section)	11.0	11.0	>7.8[a]	>5.0[a]
Horizontal (vent section)	2.2	---	---	---

[a]Because of the presence of a fracture, strains cannot be accurately measured.

volume of the capsule had decreased to the point where the capsule wall was forced outward. As the capsule wall bent outward, the iridium in that section experienced high biaxial stresses.

X. DISCUSSION

The behavior of the fueled module impacted in DIT-2 and that impacted in DIT-1 was similar. In both tests, postimpact examination revealed that the FWPF aeroshell and GISs had fractured on impact and that the GISs were slightly bowed (≈1 mm) at their midpoints. Apparently, breakup and shape change of the fuel pellet and the amount of external support determined the severity of capsule deformation. The current design, which features CBCF insulation and an open window between GISs, favors large capsule deformations by preventing significant load transfer during the early stages of deceleration. Each GIS is free to deflect at its midpoint, which allows a small area on the surface of each capsule to come in contact with the aeroshell wall earlier than the remainder of the GIS. If the fuel pellet and GIS had infinite yield strengths and the iridium clad was held tightly between them, only elastic deformation would occur on impact. Increasing the strength and rigidity of the GIS/insulator combination and eliminating all gaps in the GPHS module may reduce the severity of capsule deformation.

All microstructural and chemical analyses indicate that the iridium alloy was of good quality and reasonable reproducibility. The four capsules had similar chemistries, and all variations were within the range expected for small-lot preparations. Microhardness tests indicate that the test temperature (930°C) was low enough to permit strain hardening of the iridium alloy. Because slow postimpact cooldown is inherent with the present test array, some stress relief undoubtedly occurred, and the instantaneous strain hardening was probably higher than the hardness measurements indicate. Although the grain sizes of the DIT-2 capsules were somewhat smaller than anticipated, this discrepancy probably did not affect test outcome. The finer grained iridium alloy had substantially higher ductility than it would have possessed if the grains had reached their predicted size; that is, if the grain size had conformed to prediction, the intergranular cracking would have been more severe, and all four capsules might have breached.

Although two DIT-2 capsules breached, the impact response of all four capsules was essentially the same as the behavior of the DIT-1 capsules. Intergranular cracking occurred on the capsule walls and welds in areas of reverse bending.

The welds on all four of the DIT-2 capsules were generally of acceptable quality and contained no significant defects. The weld in capsule SR-107, however, was quite porous in the overlap region (Fig. 22). Similar porosity was observed in a wall section removed from capsule SR-105 (Fig. 23). Apparently, reheating the iridium alloy to temperatures approaching the melting point caused grain-boundary porosity in both capsules. Because such porosity appears to be a characteristic response of iridium alloy exposed to temperatures near the melting point, grain-boundary porosity is a possibility in any overlap weld.

The DIT-2 fuel pellets were chemically and microstructurally similar to one another and to the DIT-1 fuel pellets. The postimpact appearance of the iridium clads and the particle-size analysis performed on fragments removed from capsule SR-110 indicate that the impact

response of fuel pellets from both tests was qualitatively similar.

XI. CONCLUSIONS

1. DIT-2 results suggest that the impact responses of the various GPHS components are reasonably reproducible and are similar to the behavior of DIT-1 components.

2. DIT-2 findings supplement those of DIT-1. The two sets of results are not contradictory even though no capsule failures occurred in DIT-1 and two capsules breached in DIT-2. All capsules used in both tests showed significant cracking that might have propagated to failure with small increases in stress or strain.

3. The quantity of $^{238}PuO_2$ released from the two breached capsules was small (≈50 μg), but minimal increases in deformation could have increased significantly the amount released.

4. The fractures observed in the DIT-2 capsules indicate that bending stresses are very effective in producing and propagating cracks through the iridium alloy. Although the weld beads appeared to be more susceptible to cracking than the wall material, this tendency was probably a reflection of the larger grain size present in the weld beads rather than by any change in character.

5. The test temperature (930°C) was apparently low enough to permit significant strain hardening of the iridium alloy. Severely deformed areas of capsule wall had hardness values 50 to 100 points above the hardness values of undeformed wall sections.

6. A discrepancy exists between the iridium-alloy grain sizes predicted and the grain sizes observed in the DIT-1 and DIT-2 capsules.

7. The microstructures and chemical analyses of the iridium-alloy cups and welds and of the fuel pellets used in DIT-2 indicate that these components were similar to components tested in DIT-1. No structural or chemical anomalies were observed; the impact behavior of these components must be considered typical.

8. The mechanical performance of the vents in all DIT-2 capsules was satisfactory. No projection of long-term filtration capability can be made from the brief exposure to operating temperatures experienced in this test.

ACKNOWLEDGMENTS

We wish to thank J. Archuleta, L. Bergamo, and D. Pavone for their generous and excellent laboratory assistance.

REFERENCES

1. F. W. Schonfeld, "General-Purpose Heat Source Development: Safety Test Program, Postimpact Evaluation, Design Iteration Test 1," Los Alamos National Laboratory report LA-9680-SR (April 1984).

2. "Iridium Weld Inspection Data Sheet (Metallography Lab)," E. I. duPont de Nemours & Co., Savannah River Plant internal document DPSOL 235-F-PuFF-3129M, Rev. 1 (March 1981).

3. "Ultrasonic Weld Examination, GPHS Fueled Clad," E. I. duPont de Nemours & Co., Savannah River Plant procedure 235-F-PuFF-4620A, (Sept. 15, 1983).

4. A. C. Schaffhauser, "Technical Highlights of Isotope Power Materials Development at Oak Ridge National Laboratory," Oak Ridge National Laboratory report CF-79/234 (June 1979).

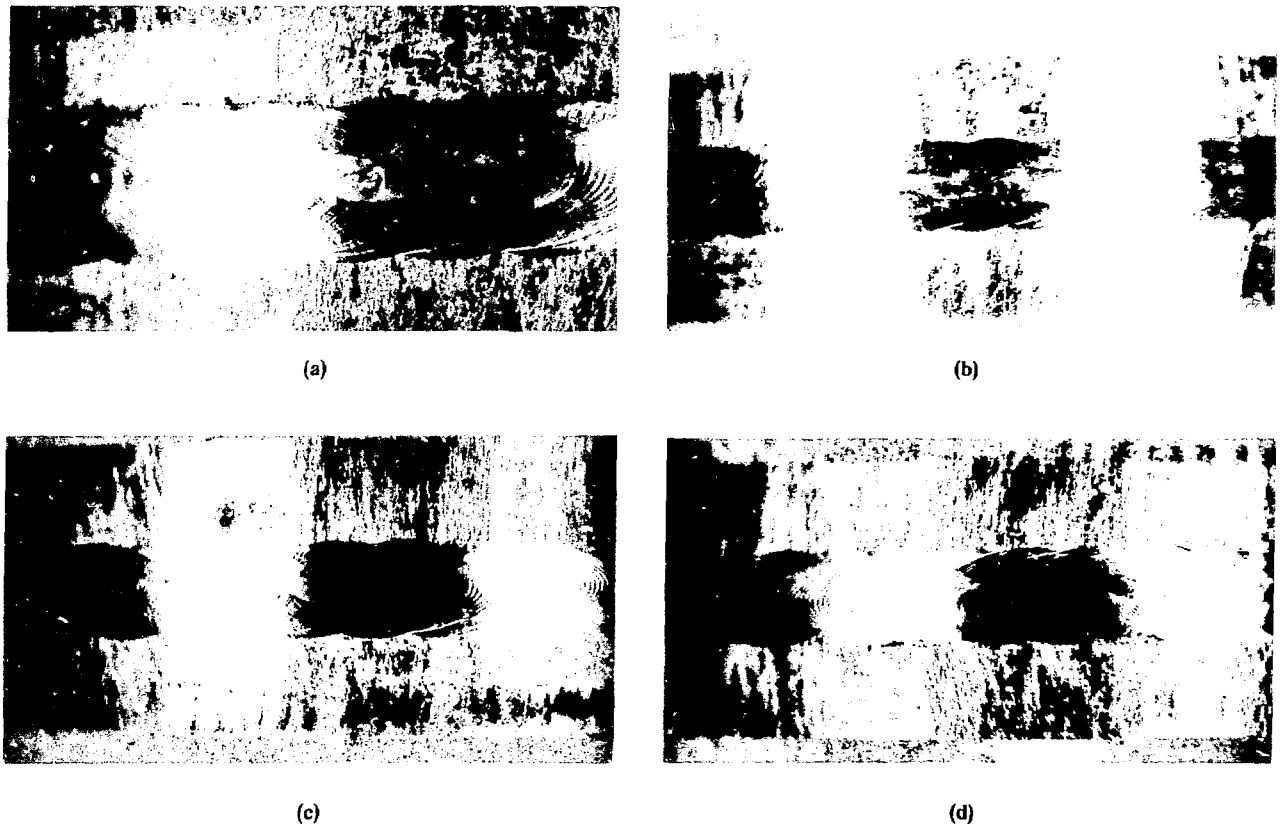

Fig. 1. Weld overlaps of the DIT-2 capsules. (a) SR-105, 8X; (b) SR-106, 5X; (c) Sr-107, 5X; and (d) SR-110, 5X.

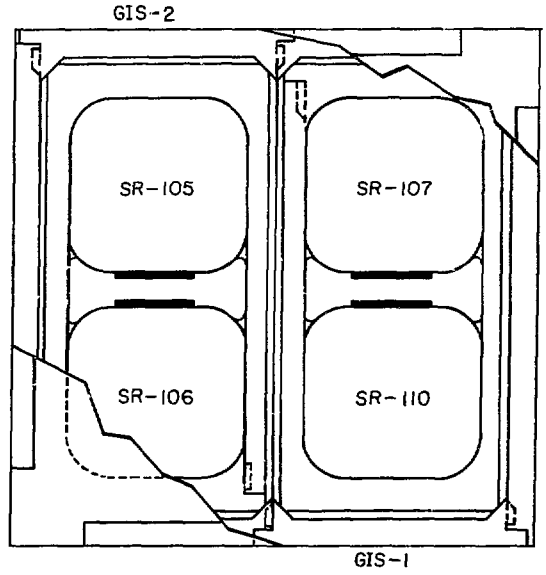

Fig. 2. DIT-2 test positions (plane view of impact face).

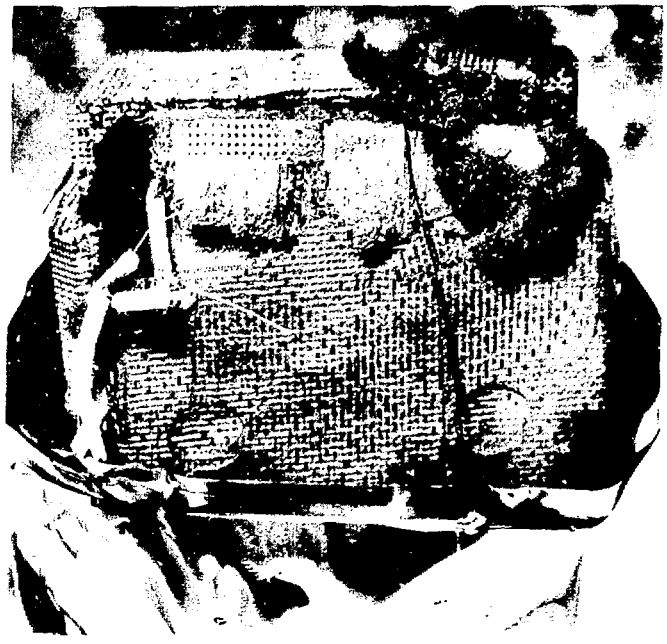

(a)

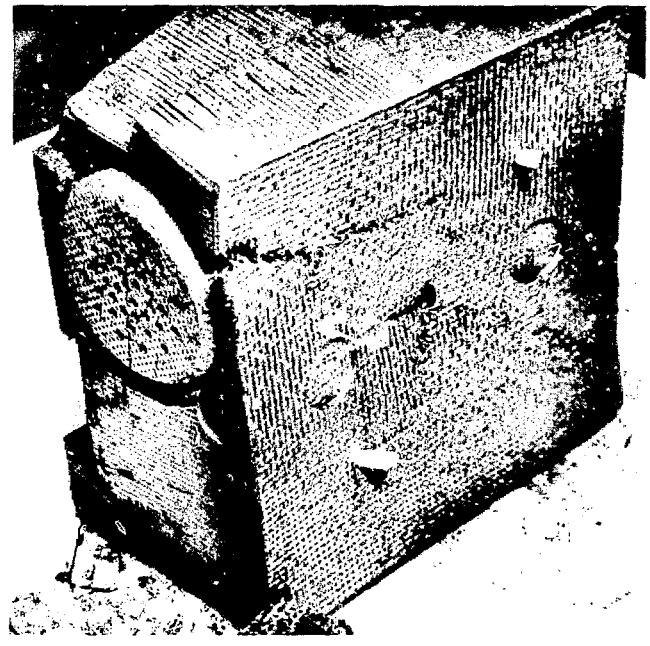

(b)

Fig. 3. The re-entry shell used in the DIT-2 impact. (a) Impact face of the module, still contained within the radiation shields, 0.6X, and (b) back face of the module, 0.45X.

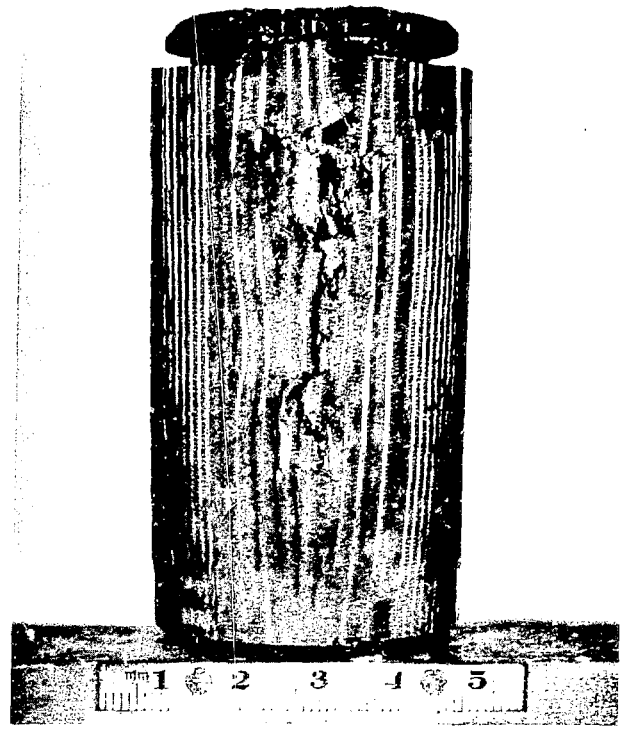

(a)

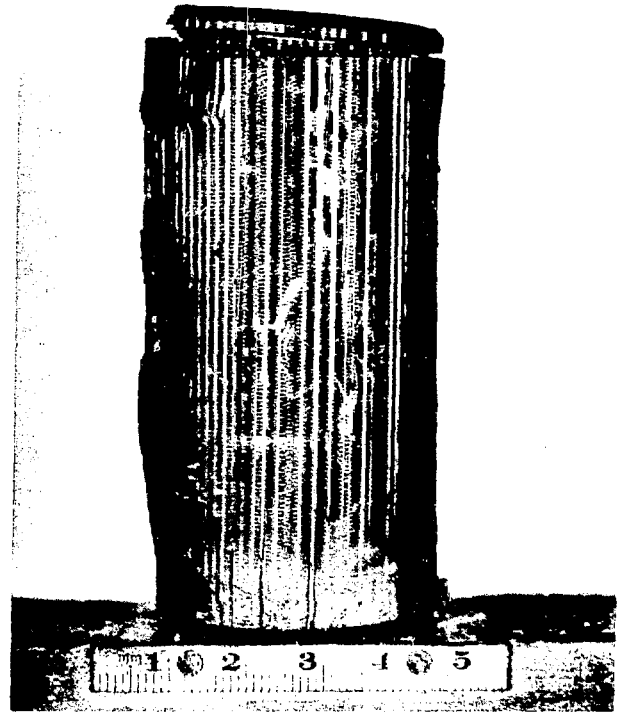

(b)

Fig. 4. GIS-1, containing fueled clads SR-107 and SR-110. (a) Impact face and (b) side view with impact face to the left.

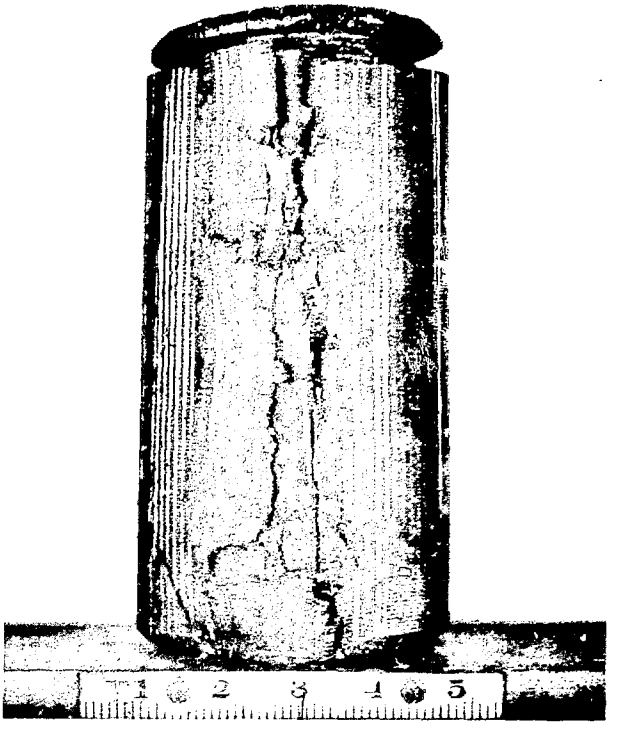

(a)

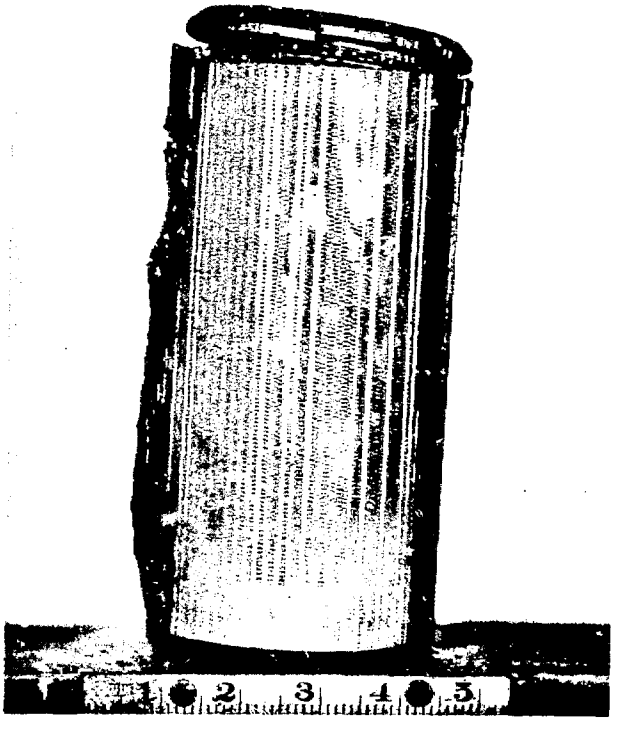

(b)

Fig. 5. GIS-2, containing fueled clads SR-105 and SR-106. (a) Impact face and (b) side view.

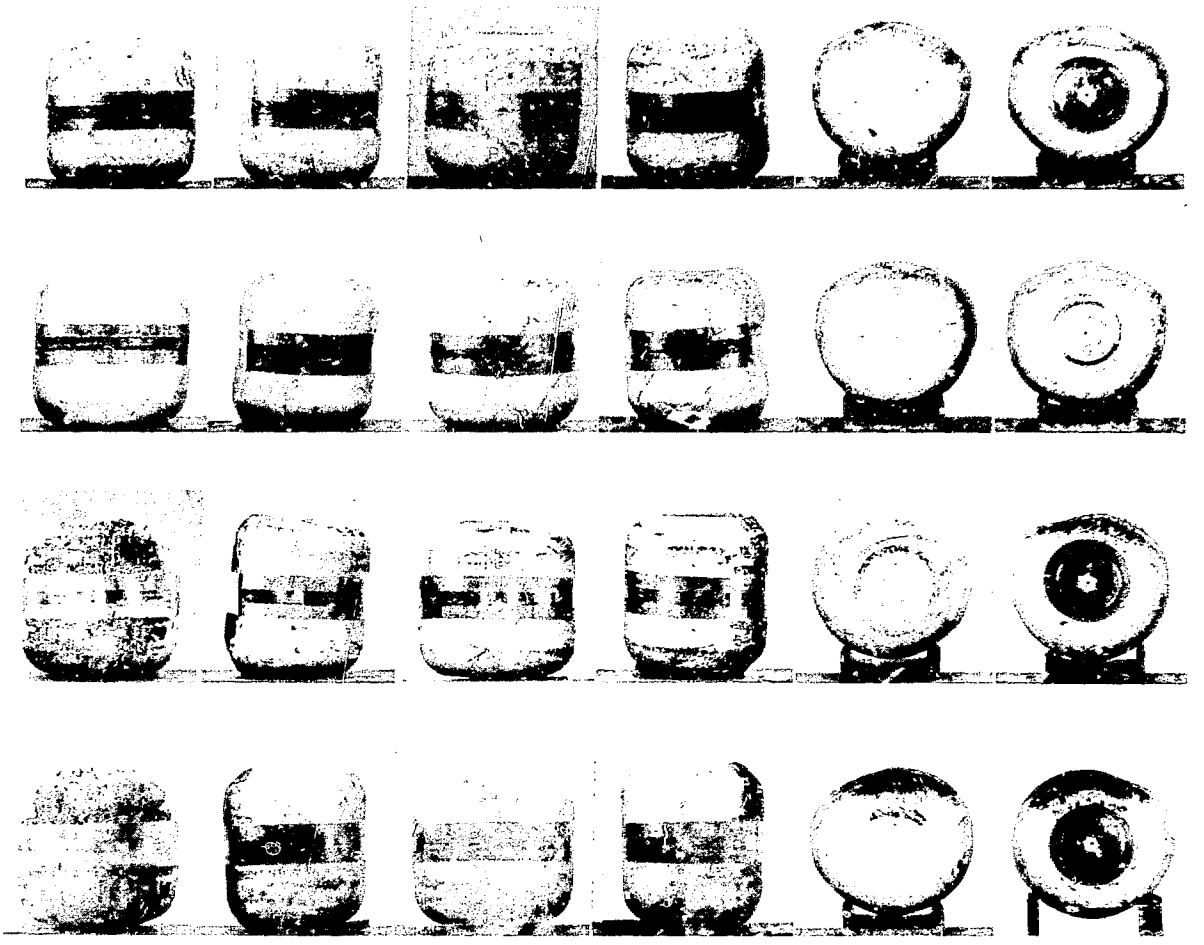

Fig. 6. The DIT-2 fueled clads after impact at 58 m/s and 930°C. The impact face is at the left of each row, and the clad is rotated 90° in each succeeding view. The vented and blind ends complete the rows. All 0.7X.

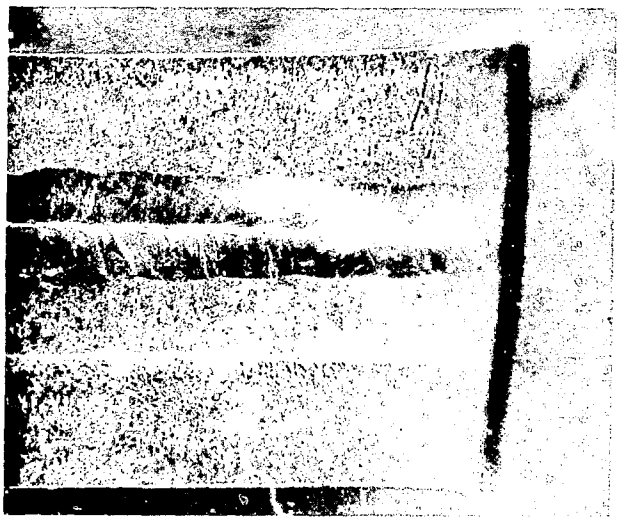

Fig. 7. Cracked inner surface of the closure weld on capsule SR-105. 20X.

Fig. 8. Cracks in the wall of capsule SR-105 adjacent to the weld bead. 50 X.

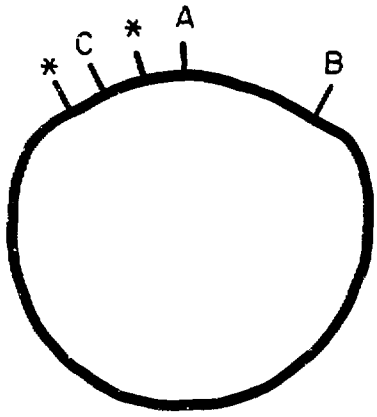

(a)
SR-105

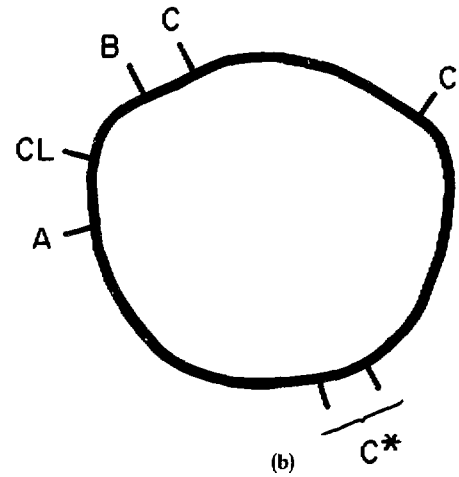

(b)
SR-106

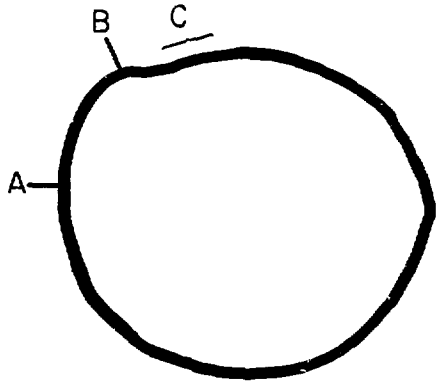

(c)
SR-107

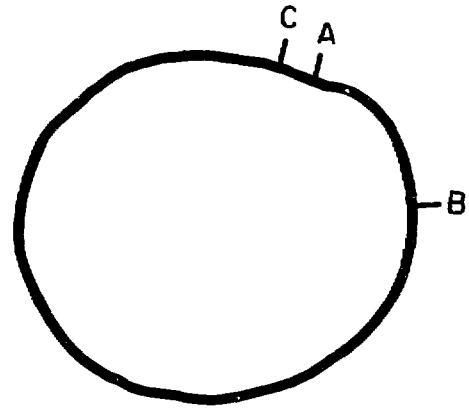

(d)
SR-110

Symbol	Definition
A	Weld submergence
B	Weld terminus
C	Cracks
*	Ultrasonic indication of a weld defect
CL	Centerline crack

Fig. 9. Features of the impacted DIT-2 capsule welds. The locations of the weld submergence, terminus, and cracking were determined by macroscopic inspection; ultrasonic indication of defects was provided by the Savannah River Plant.

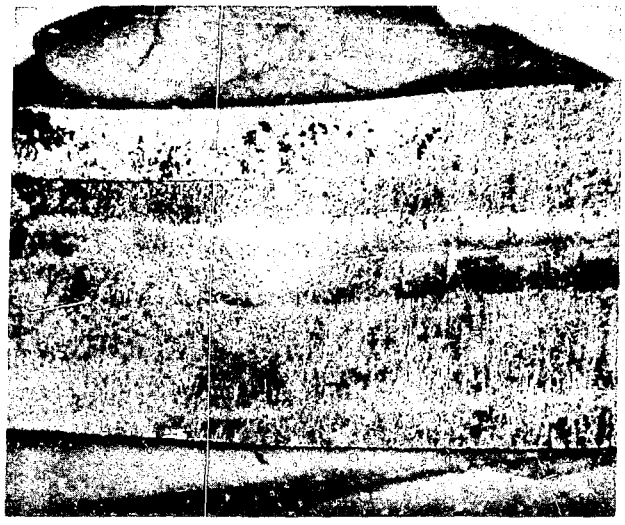

(a)

(b)

(c)

Fig. 10. Three crack families were observed on the interior of capsule SR-106. (a) In the reverse-bend region nearest the weld overlap; (b) on the second reverse bend; and (c) on the capsule back. All 6X.

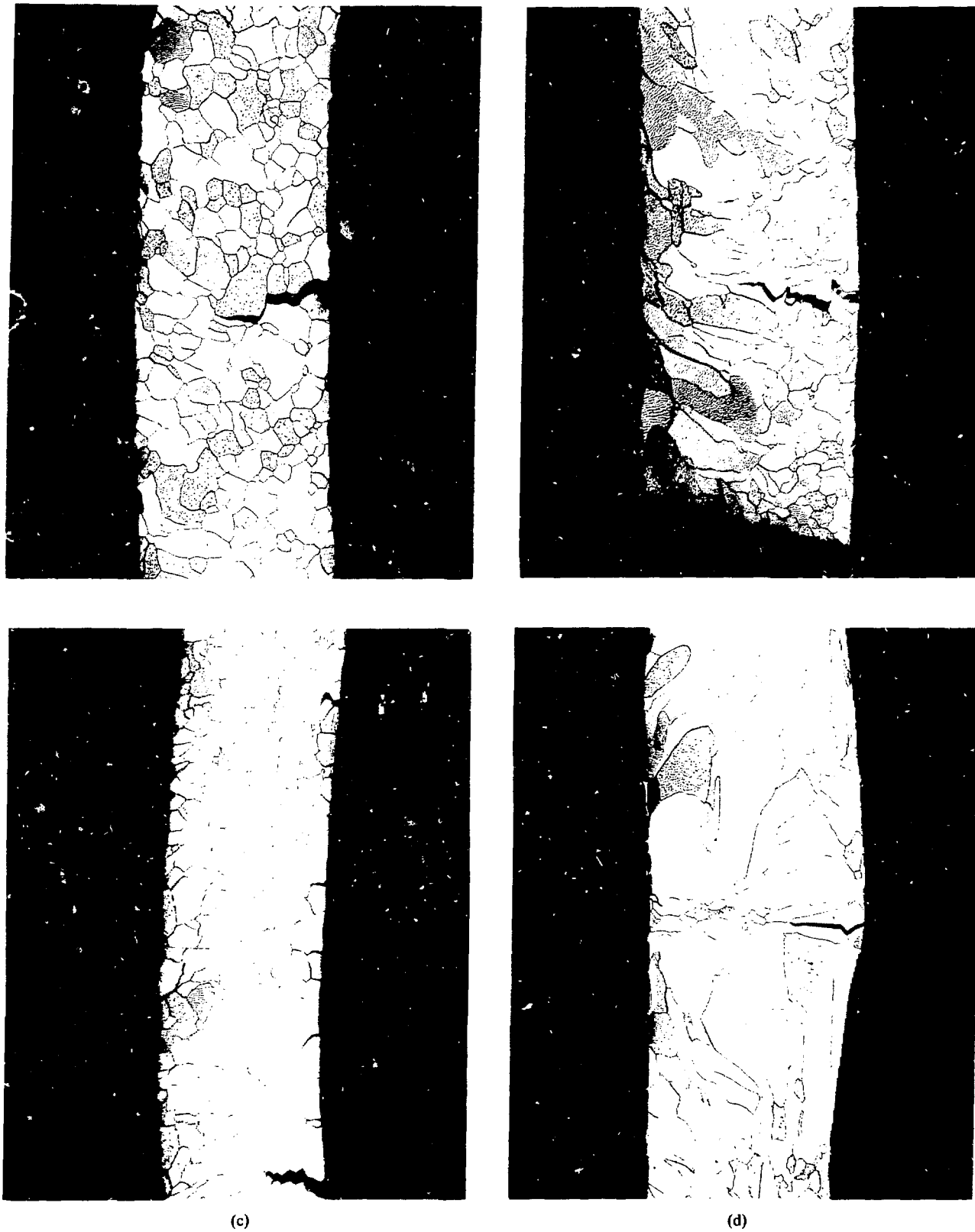

(c) (d)

Fig. 11. Microstructural features of the cracks seen in Fig. 10. (a) Largest weld bead crack at the first reverse bend, (b) largest crack at the second reverse bend, (c) trailing face of the SR-106 capsule, and (d) centerline crack at the weld overlap. All 50X.

Fig. 12. Severe internal cracking present at the reverse bend in capsule SR-107, 6X.

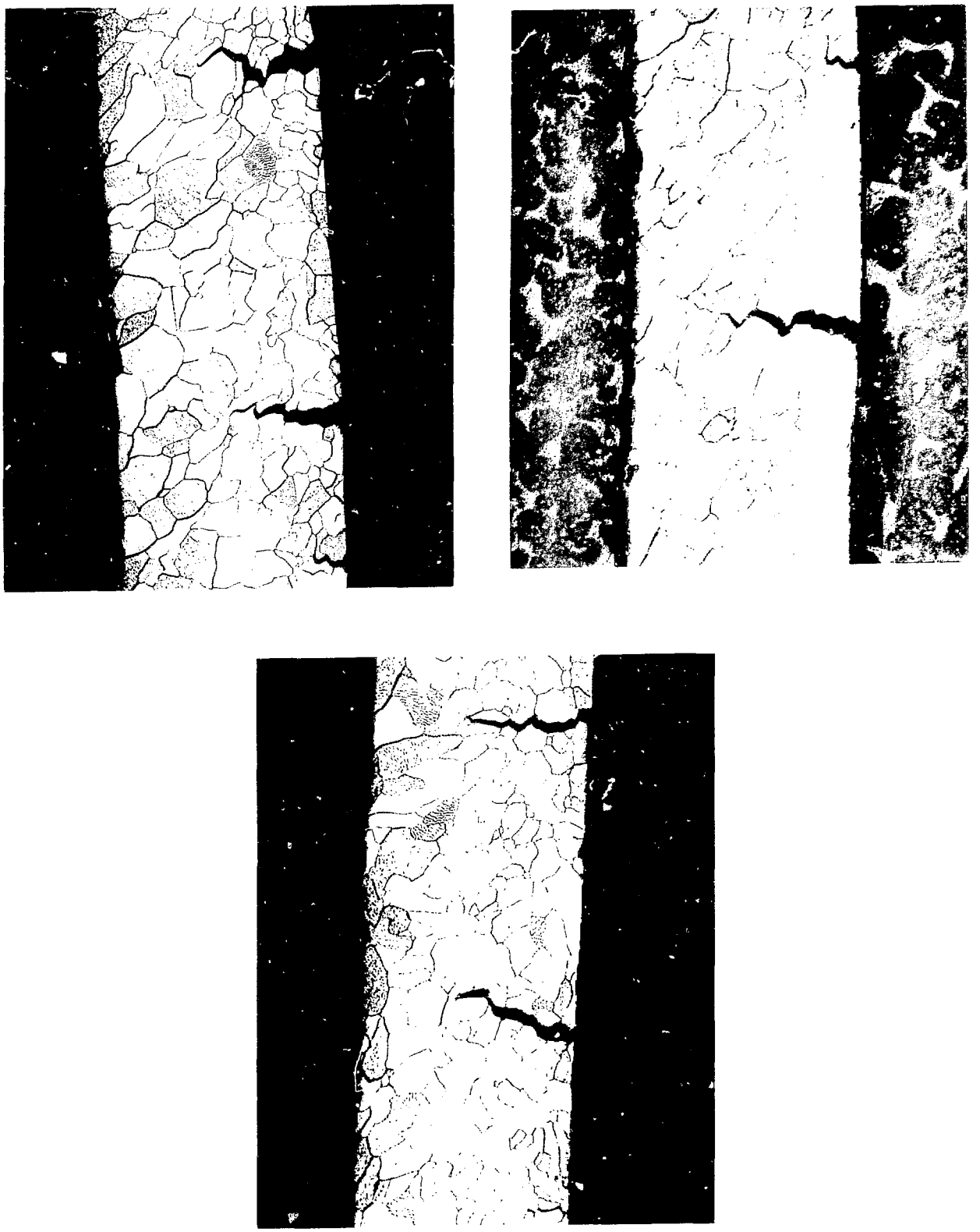

Fig. 13. Cross section containing the cracks seen in Fig. 12. 50X.

(a)

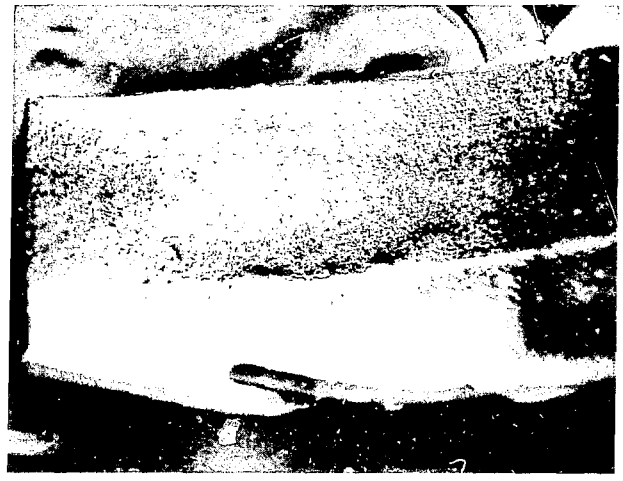

(b)

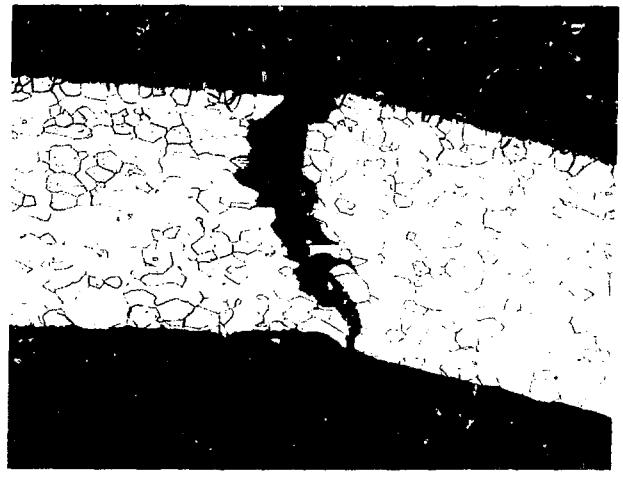

(c)

Fig. 14. Breach in the vent-end radius of capsule SR-107. (a) External surface, 6X; (b) internal surface, 6X; and (c) micrograph of a section perpendicular to the crack, 50X.

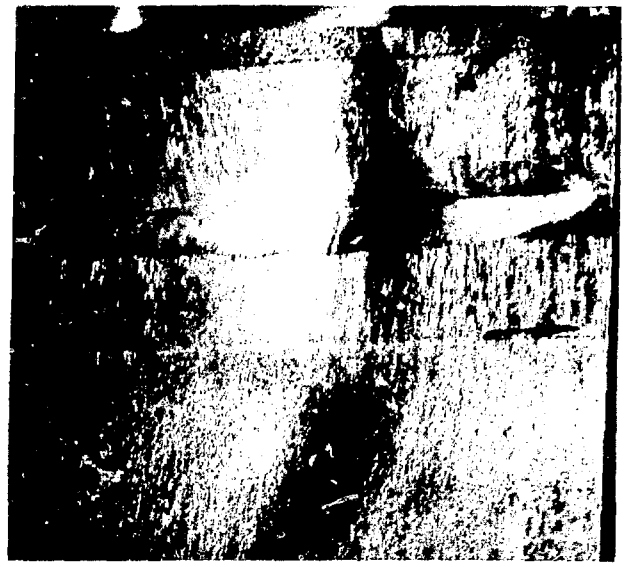

(a)

(b)

Fig. 15. (a) Only a few internal cracks were observed in the reverse bend region of capsule SR-110, 6X. (b) The deepest weld crack penetrated over 50% of the wall thickness, 100X.

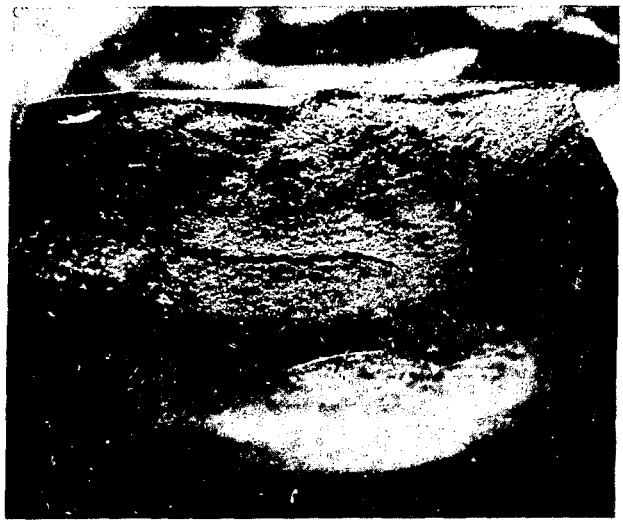

(a)

(b)

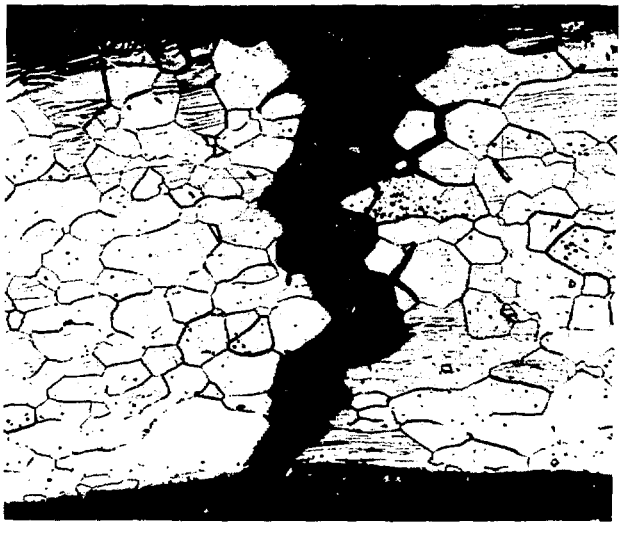

(c)

Fig. 16. Breach in the vent-end radius of capsule SR-110. (a) External surface, 6X; (b) internal surface, 6X; and (c) etched cross section, 100X.

(a)

(b)

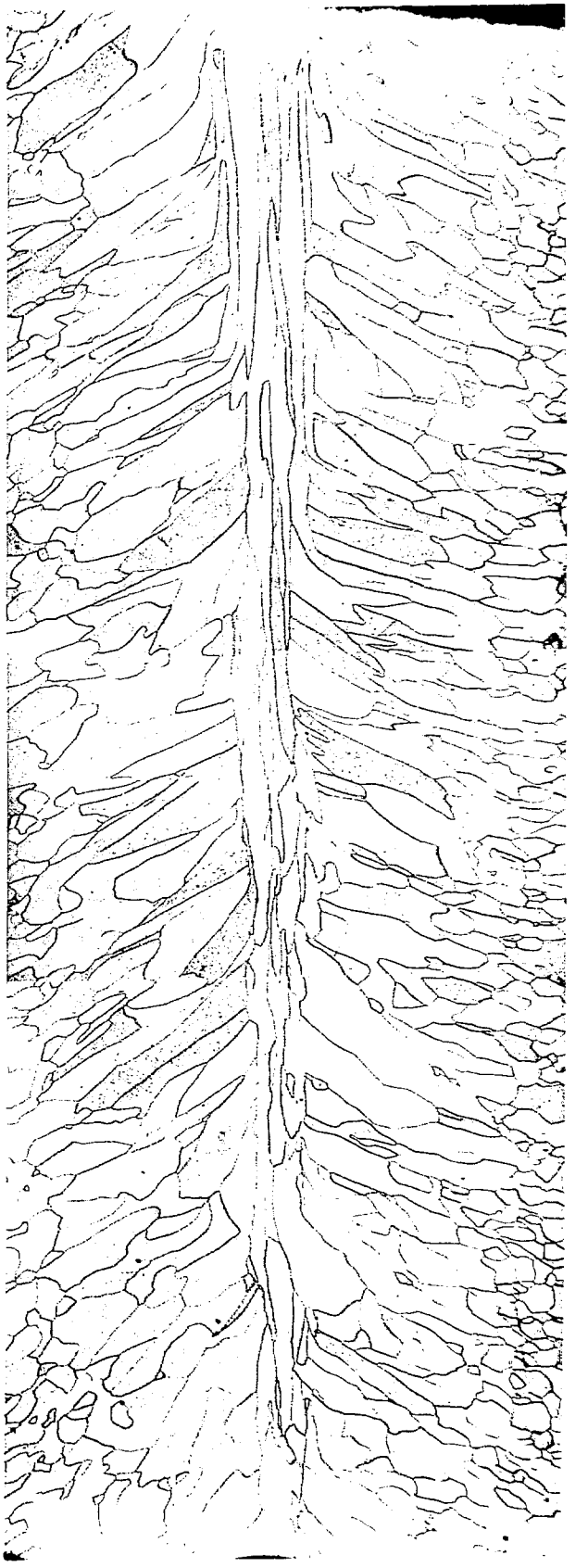

(c)

Fig. 17. The microstructures of the closure weld in capsule SR-105 were typical of Savannah River welds. (a) Single-pass region, 50X; (b) overlap region, 40X; and (c) face-on section, 40X.

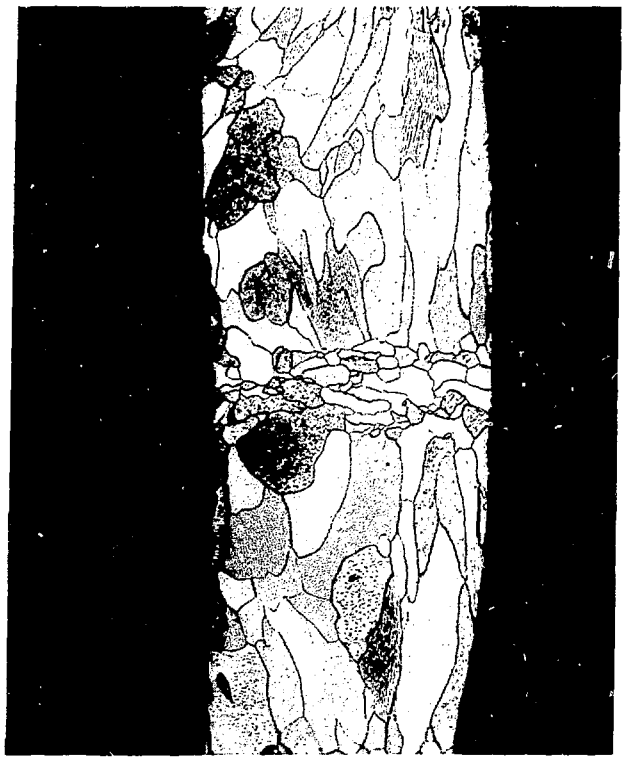

Fig. 18. Typical microstructure observed in the single-pass weld section removed from capsule SR-106, 50X.

Fig. 19. The centerline crack observed in the overlap region of SR-106 penetrated over 30% of the wall thickness, 50X.

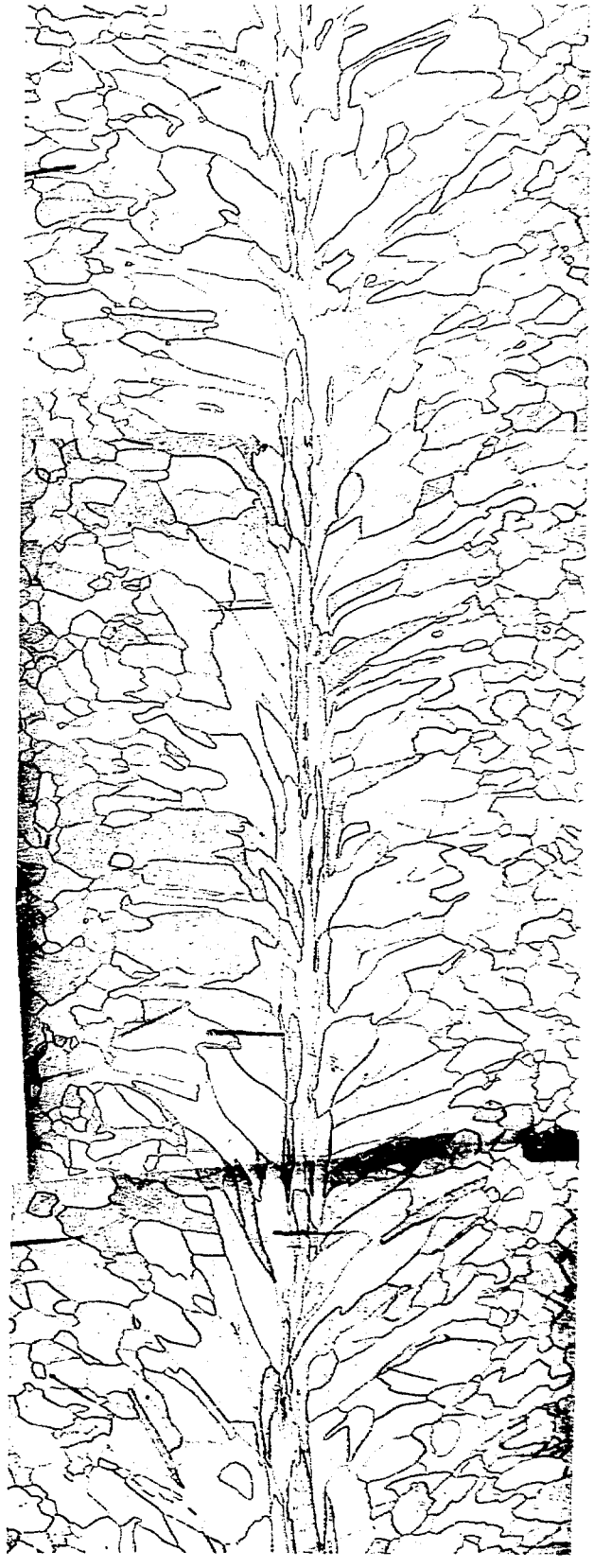

Fig. 20. The closure weld of capsule SR-106 exhibited the expected microstructure in the face-on region, 40X.

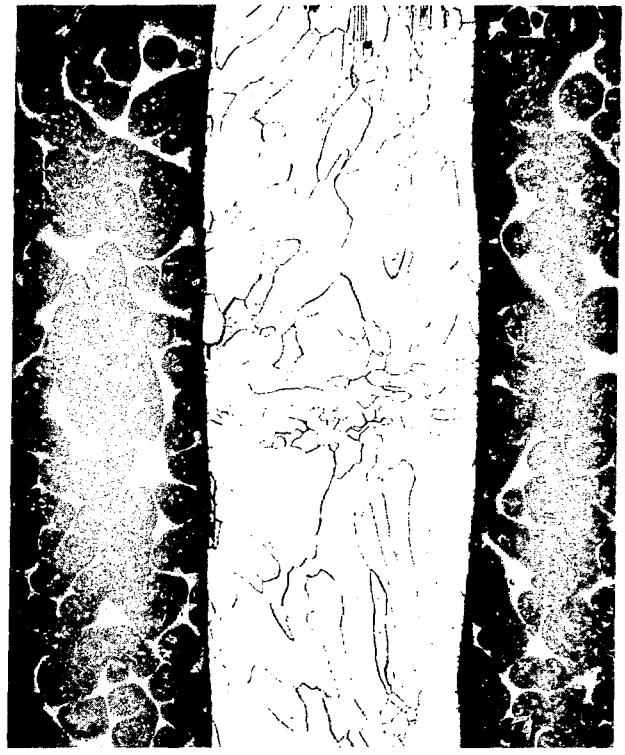

Fig. 21. The microstructure of the single-pass weld specimen taken from capsule SR-107 was normal, 50X.

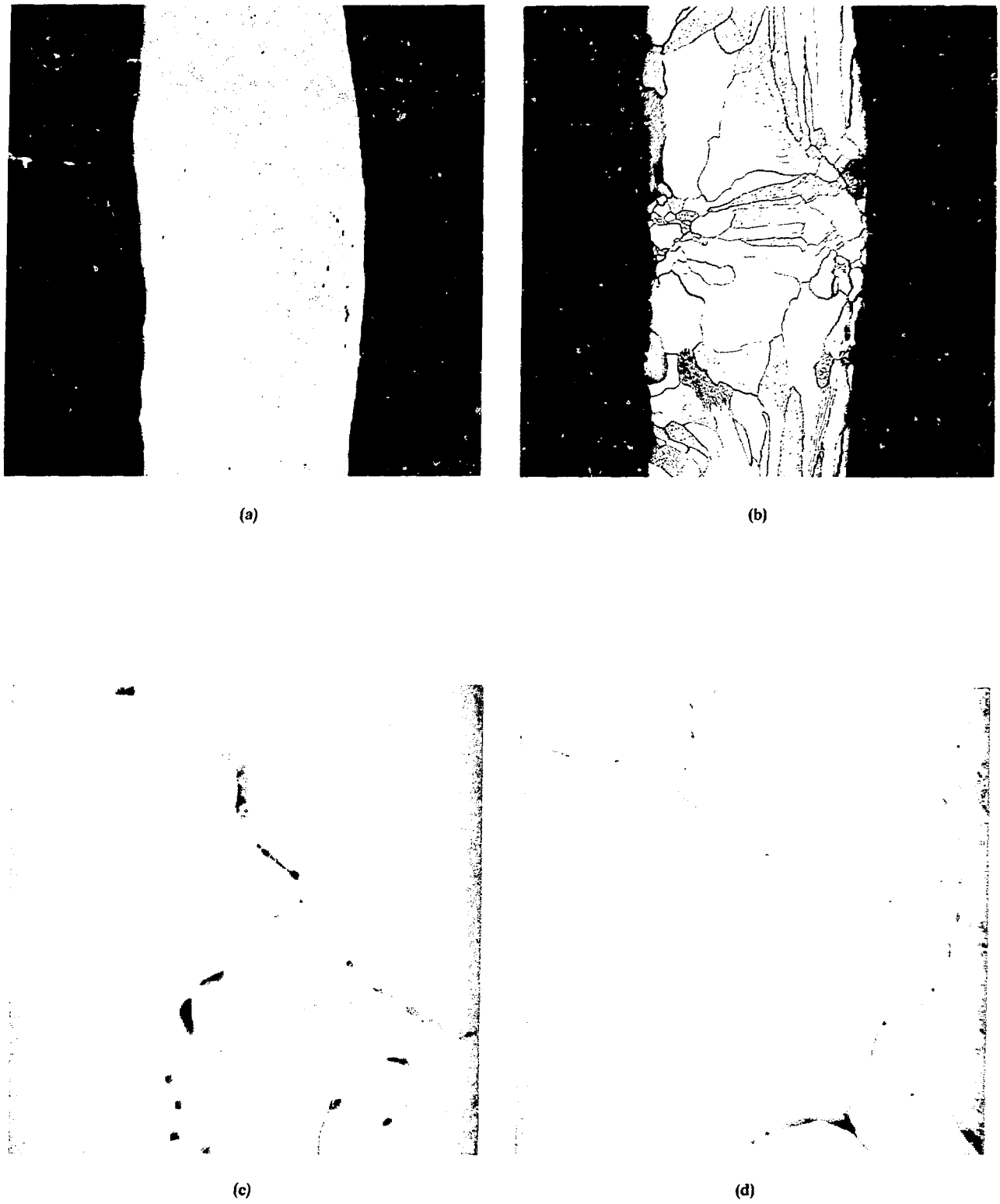

Fig. 22. Porosity was present in the overlap region of the SR-107 weld. (a) As-polished, 50X; (b) same area, etched, 50X; (c) SEM photograph of porosity in the central portion of the weld bead, 700X; and (d) SEM photograph of porosity at the root of the weld bead, 700X.

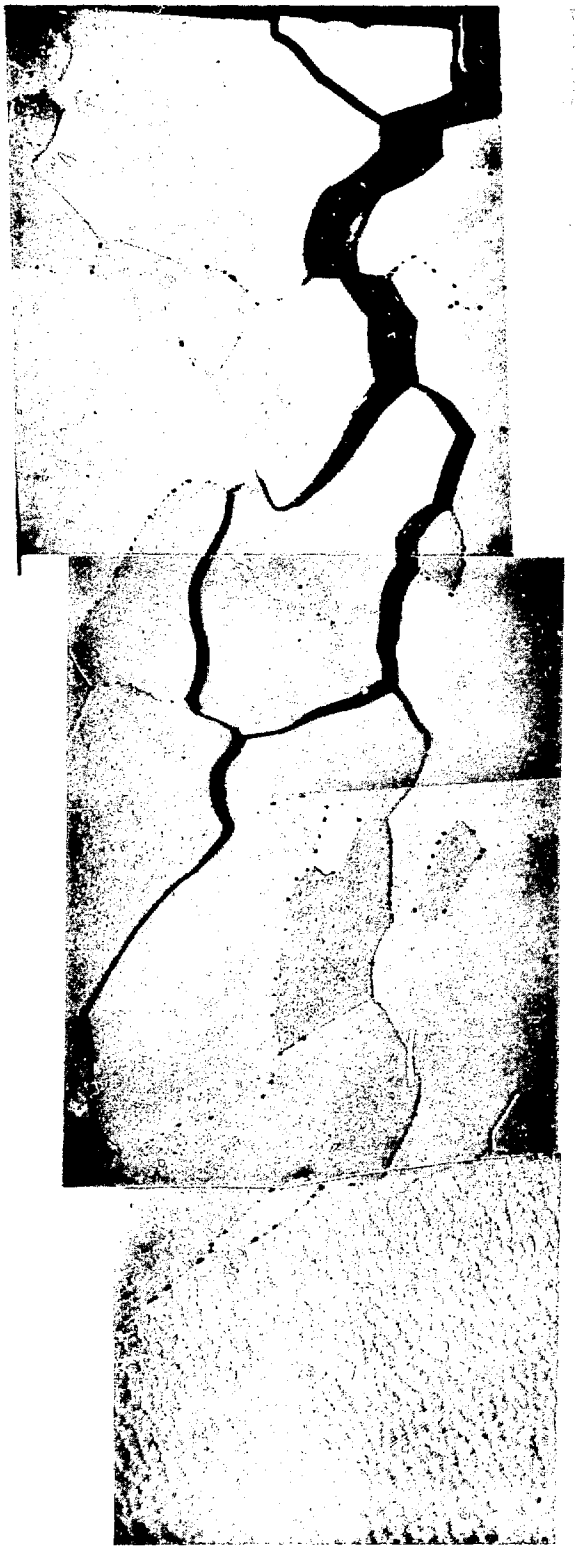

Fig. 23. The base metal adjacent to the weld in capsule SR-105 contained grain-boundary porosity, 300X.

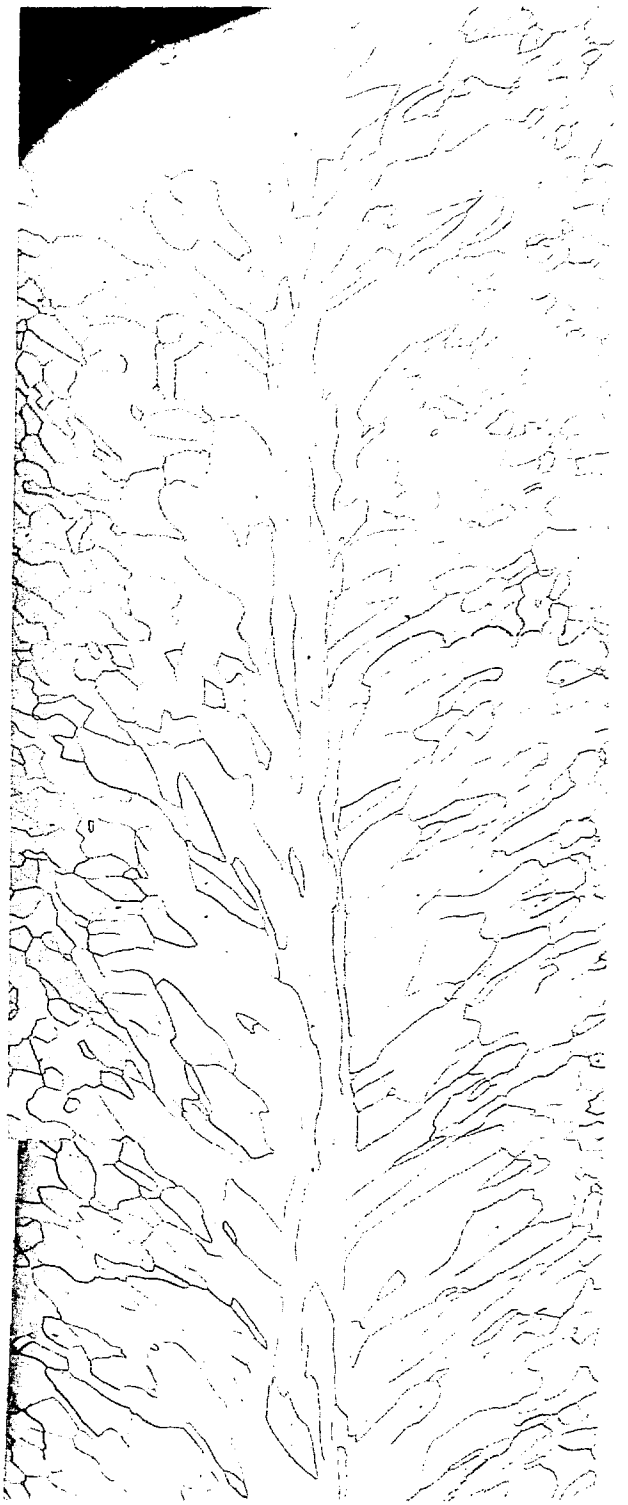

Fig. 24. Face-on section of the single-pass weld in capsule SR-107, 40X.

Fig. 25. The single-pass specimen removed from capsule SR-110 was normal, 50X.

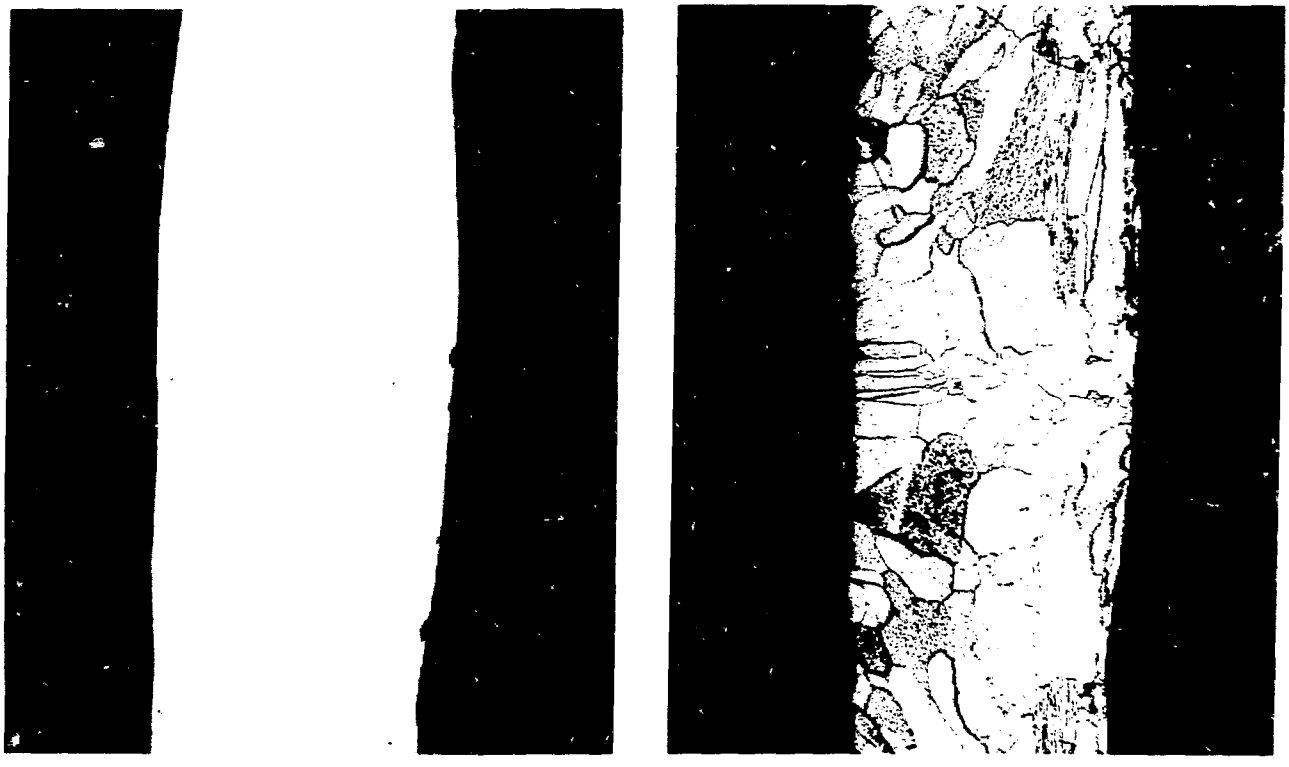

(a) (b)

Fig. 26. A few small pores were observed in the overlap weld sample taken from capsule SR-110; otherwise, the section exhibited typical microstructure. (a) As-polished and (b) etched. Both 50X.

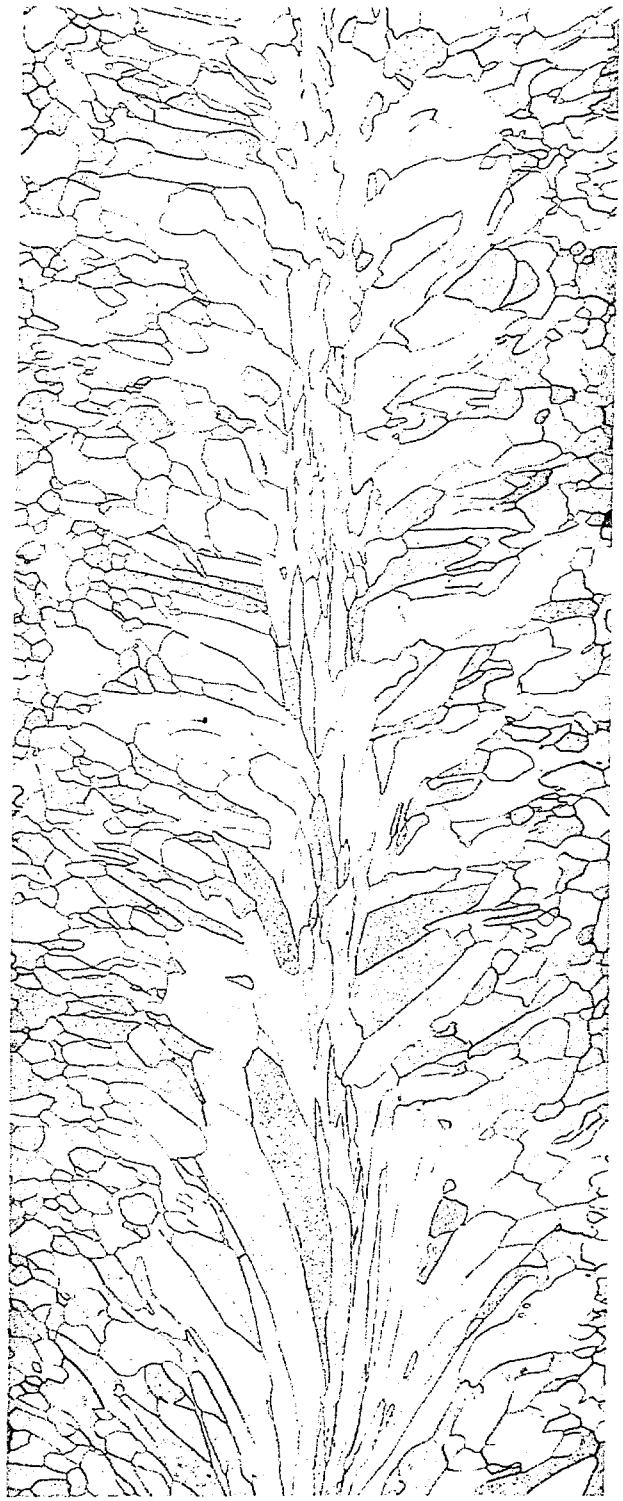

Fig. 27. The face-on weld section removed from SR-110 had a typical microstructure, 40X.

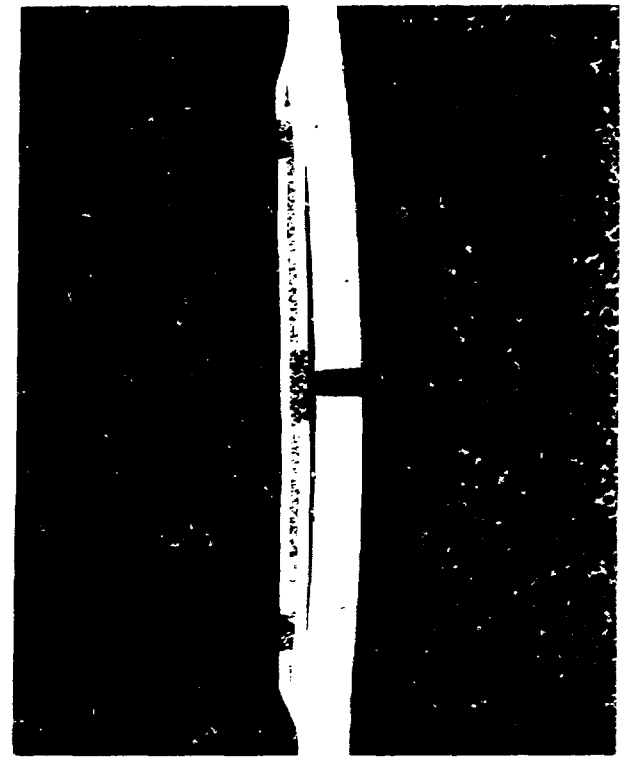

Fig. 28. A vertical section through the capsule SR-105 vent, 10X.

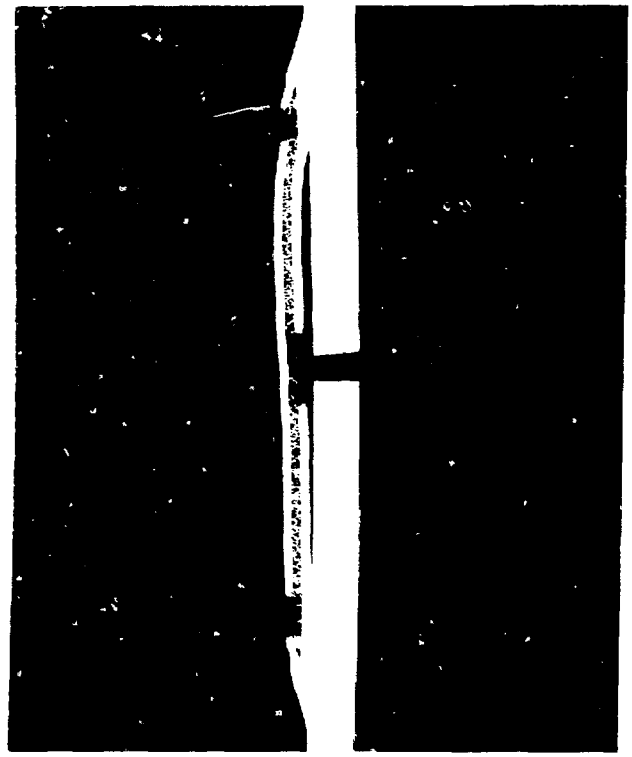

Fig. 29. The capsule SR-106 vent exhibited a small amount of plastic strain, 10X.

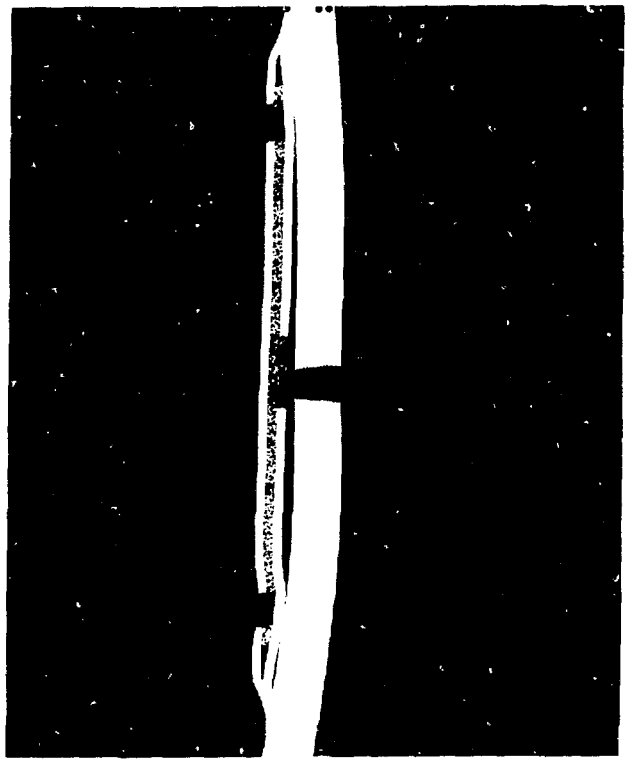

Fig. 30. The capsule SR-107 vent exhibited the same type of deformation as that in the SR-106 vent, 10X.

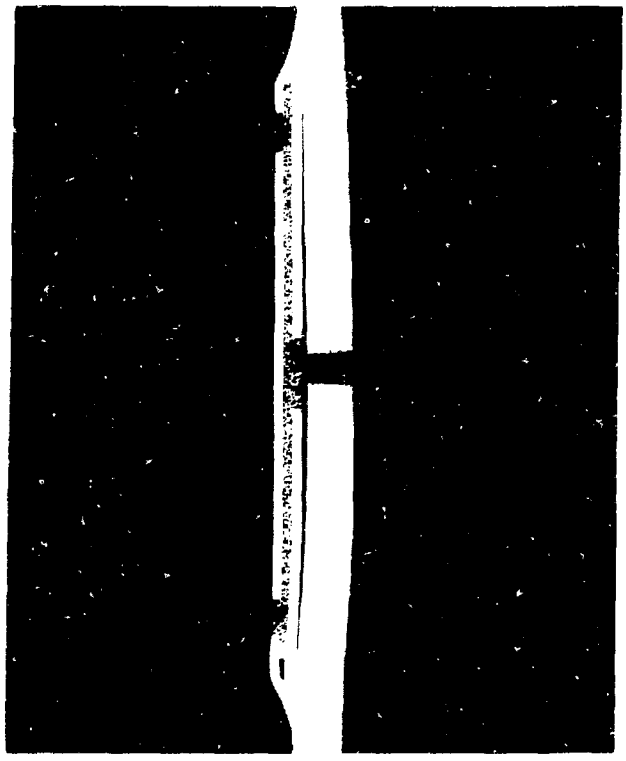

(a)

(b)

(c)

Fig. 31. A small crack was present in the capsule SR-110 vent-assembly weld. (a) As-polished, 10X; (b) as-polished, 100X; and (c) etched, 40X.

(a)

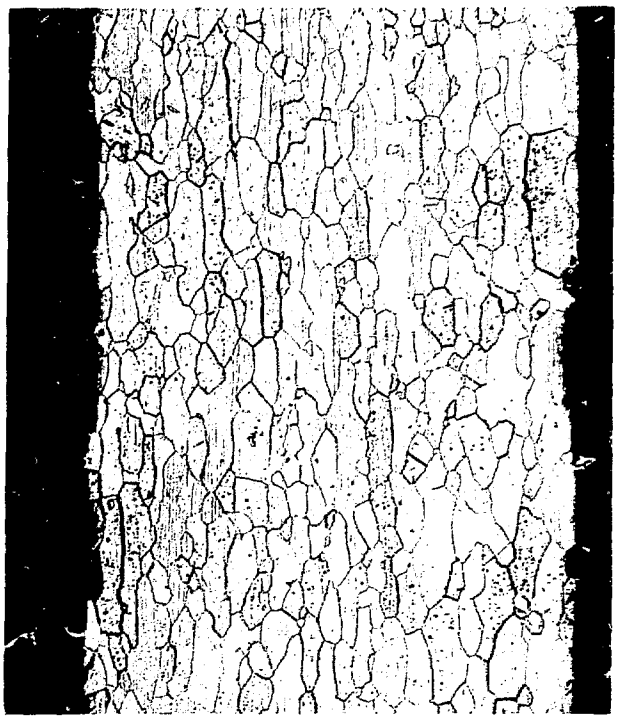

(b)

(c)

Fig. 32. Microstructures of wall samples taken from capsule SR-105. Polished and etched. (a) Weld-shield cup, (b) vent cup, and (c) deformed portion of vent cup wall. All 100X.

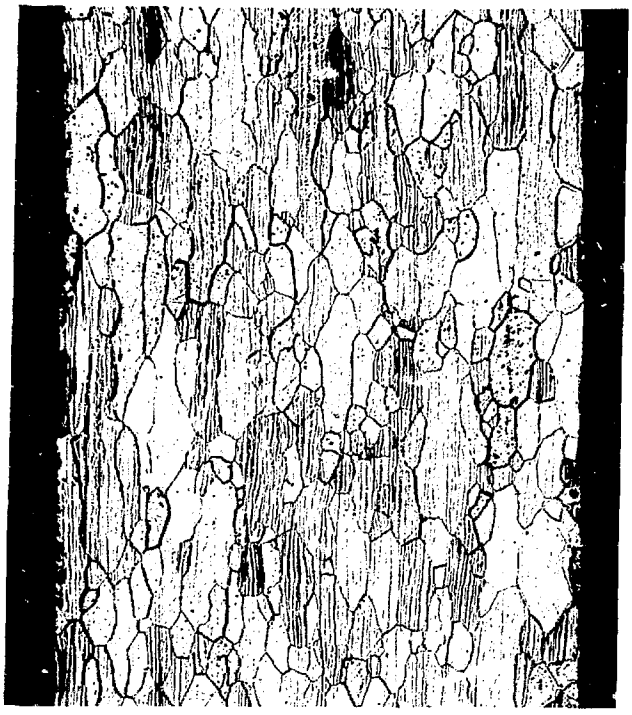

(a)

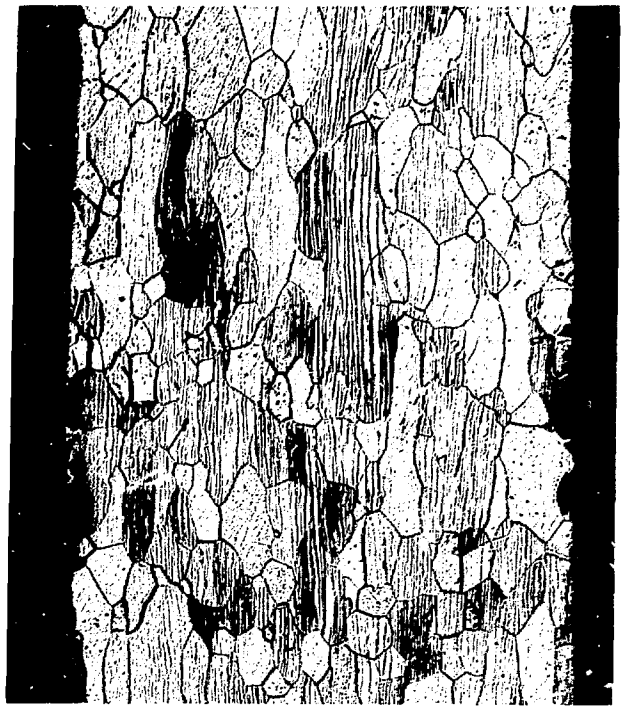

(b)

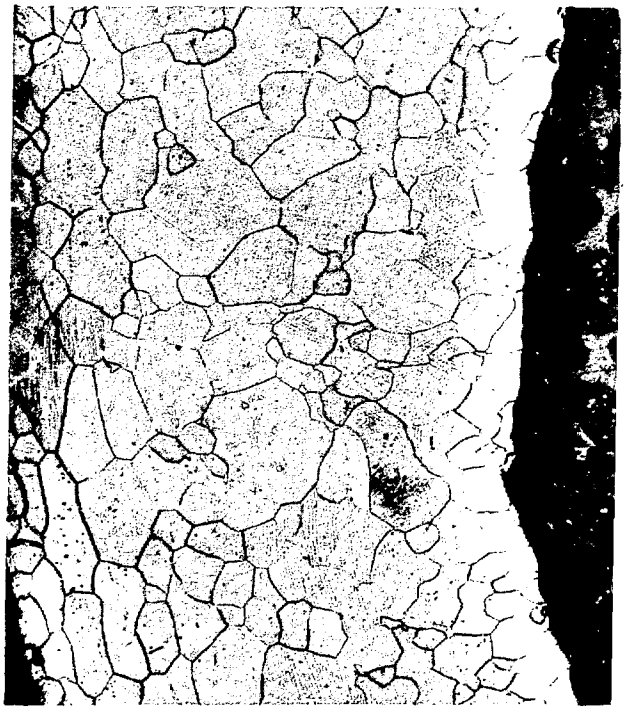

(c)

Fig. 33. Microstructures of wall samples taken from capsule SR-106. Polished and etched. (a) Weld-shield cup, (b) vent cup, and (c) deformed portion of vent cup wall. All 100X.

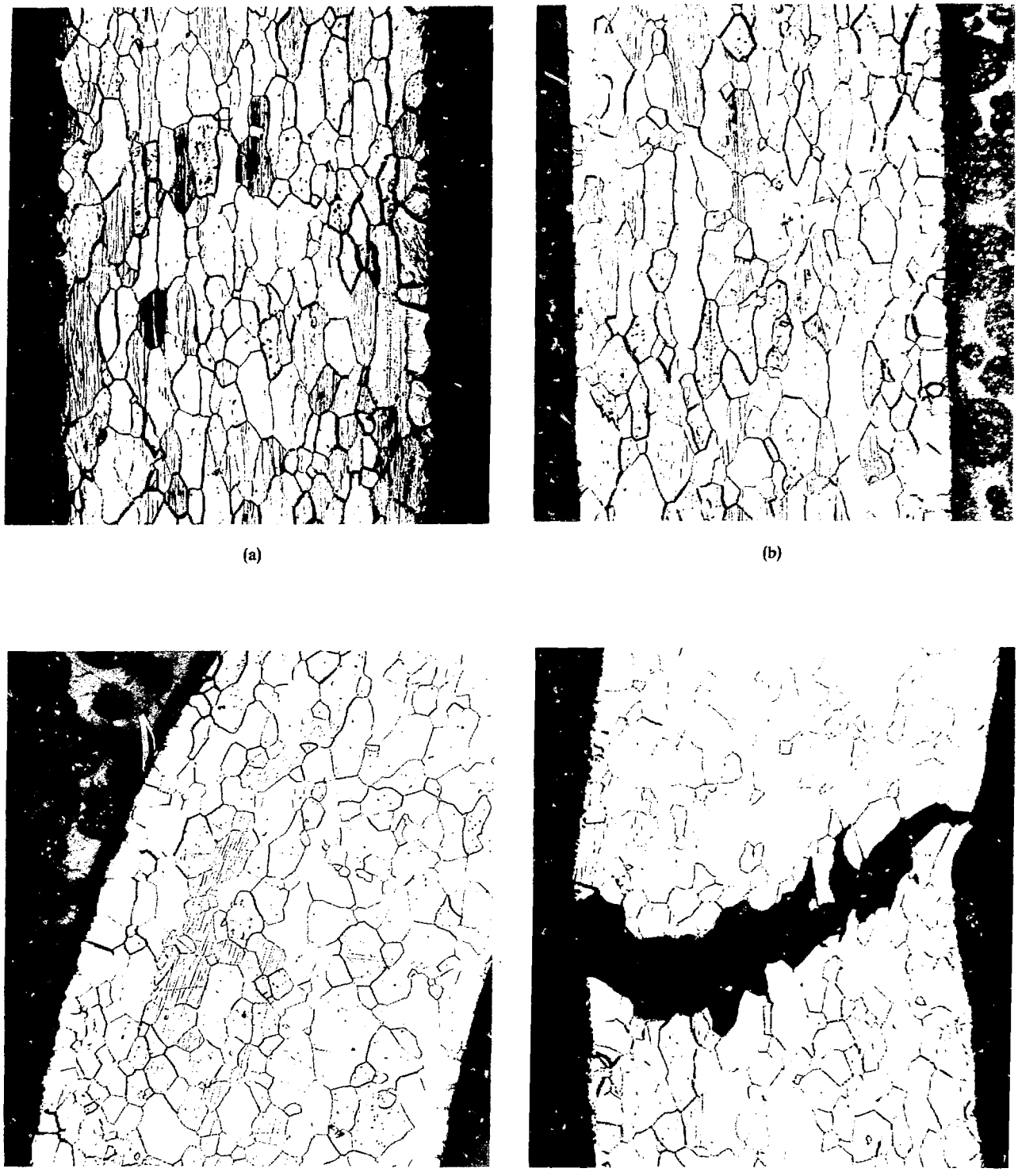

Fig. 34. Microstructures of wall samples removed from capsule SR-107. Polished and etched. (a) Weld-shield cup, (b) vent cup, (c) deformed portion of vent cup wall, and (d) vent cup section containing the breaching crack. All 100X.

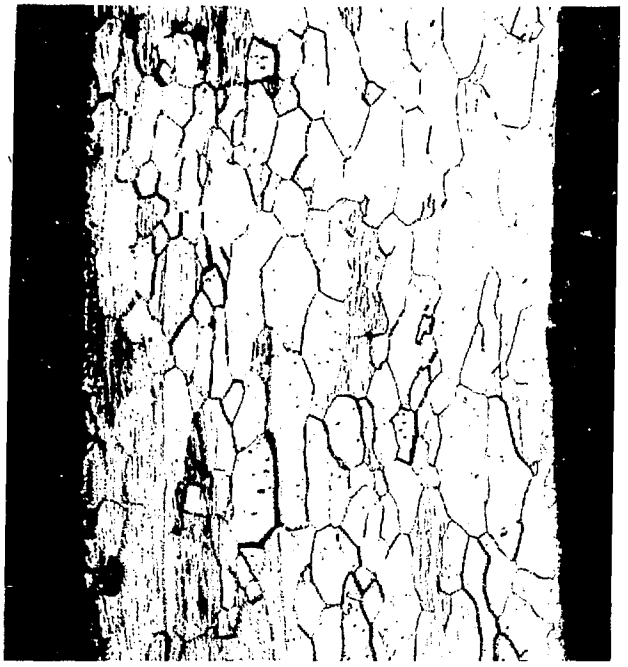

(a)

(b)

(c)

Fig. 35. Microstructures of wall samples removed from SR-110. Polished and etched. (a) Weld-shield cup, (b) vent cup, and (c) vent cup section containing the breaching crack. All 100X.

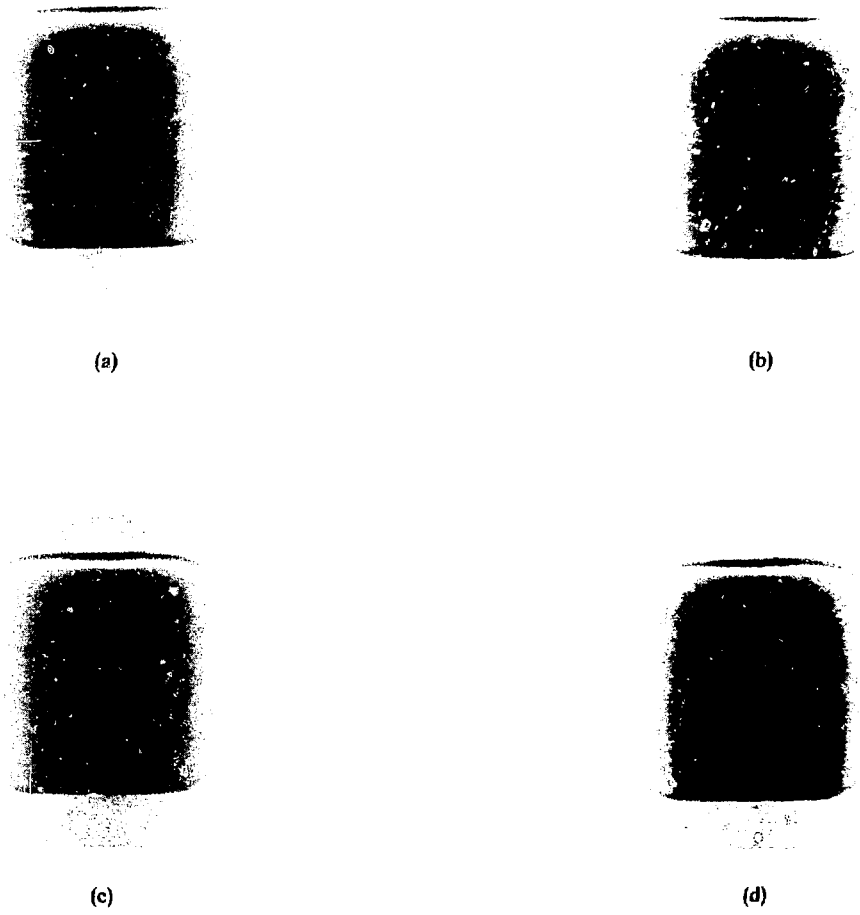

Fig. 36. Contact prints made from radiographic negatives of encapsulated fuel pellets used in DIT-2. (a) Fuel pellet SR-105, (b) pellet SR-106, (c) pellet SR-107, and (d) pellet SR-110.

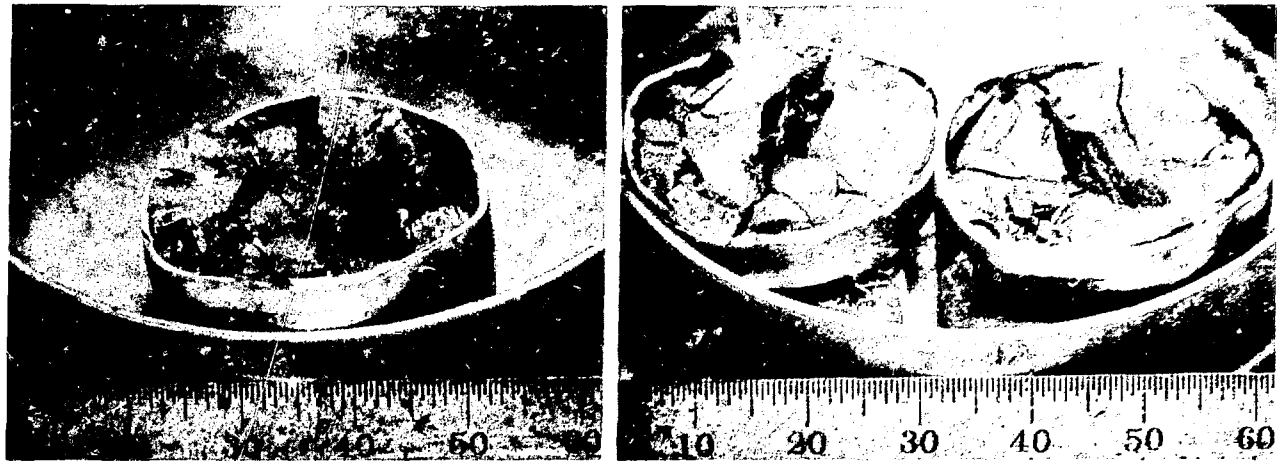

(a) (b)

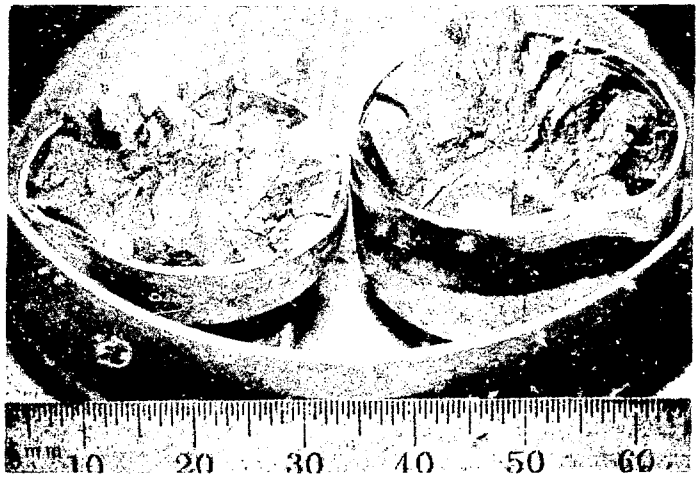

(c)

(d)

Fig. 37. Macrographs of opened DIT-2 capsules, illustrating the patterns of fuel breakup. (a) SR-105, (b) SR-106, (c) SR-107, and (d) SR-110. All 1.5X.

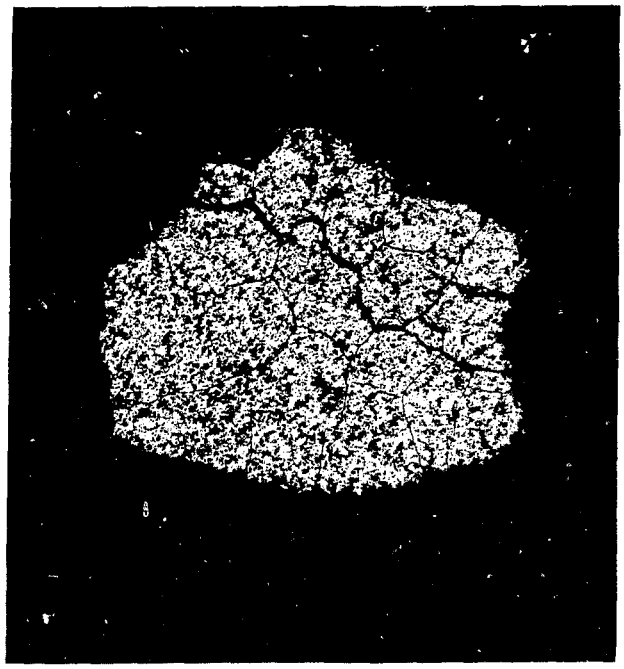

(a)

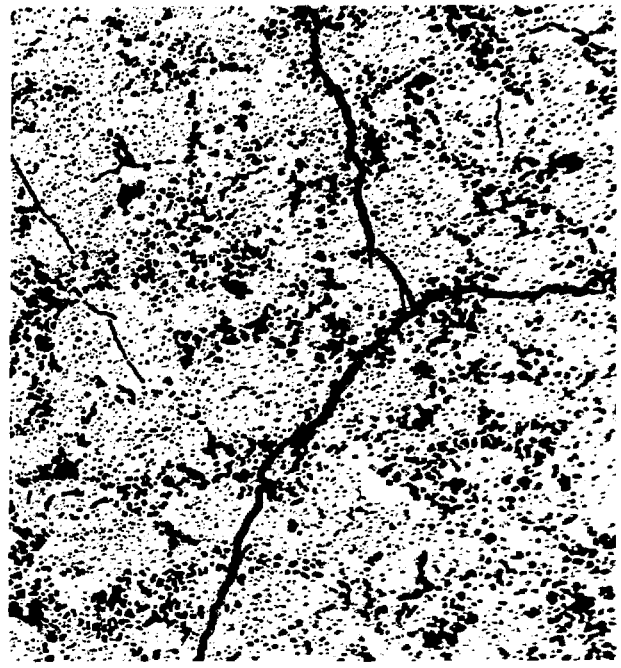

(b)

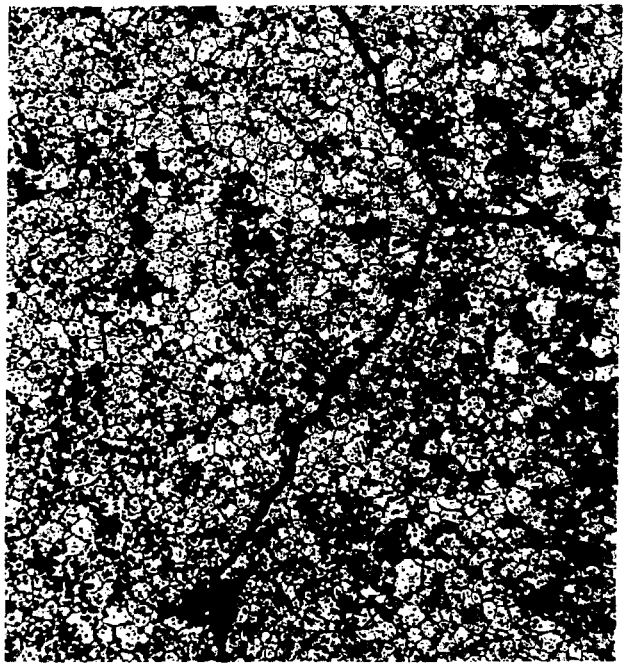

(c)

Fig. 38. Ceramographic specimen obtained from the central portion of fuel pellet SR-105. (a) Macrograph, as-polished, 10X; (b) micrograph, as-polished, 100X, and (c) etched, 100X.

(a)

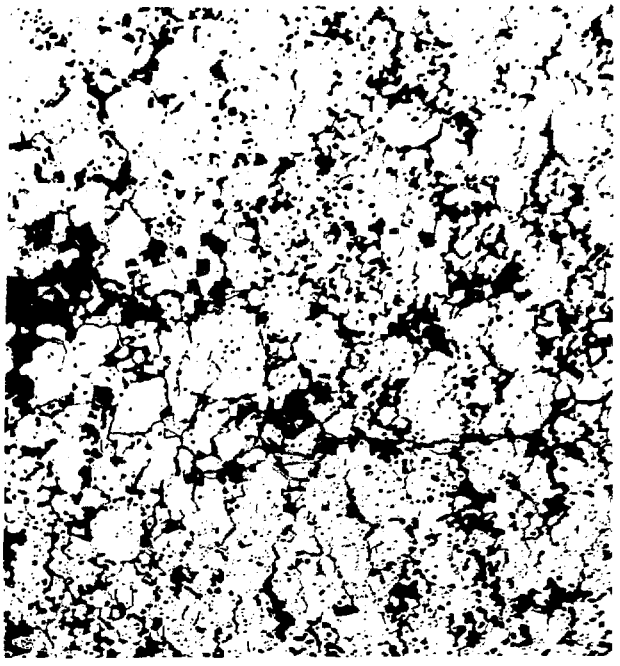

(b)

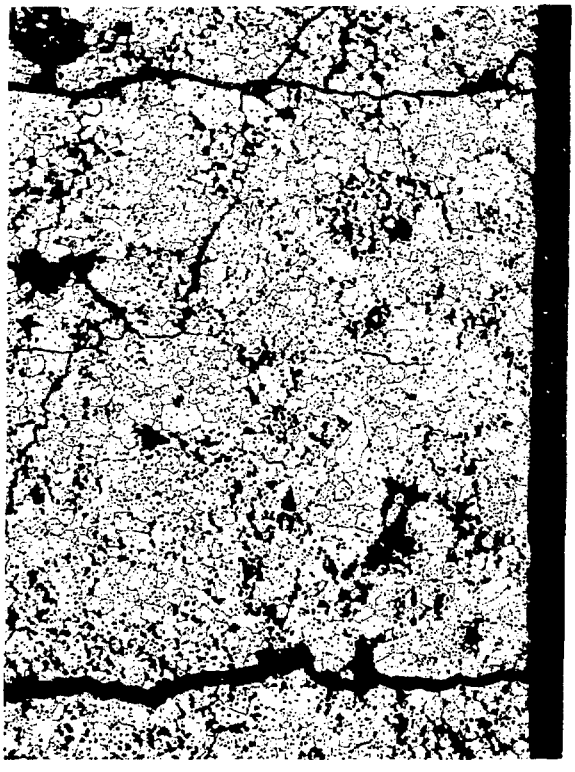

(c)

Fig. 39. Ceramographic specimen obtained from the external portion of SR-105. (a) Macrograph, as-polished, 9X; (b) micrograph, as-polished, 100X; and (c) etched, 100X.

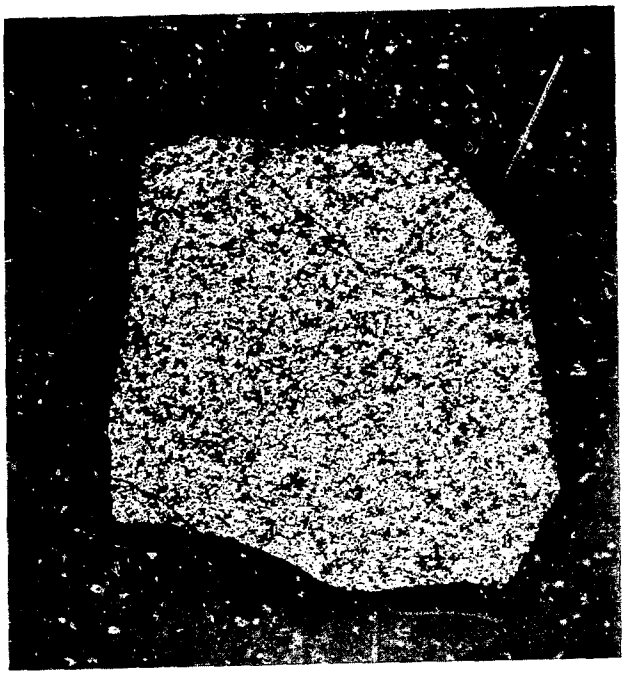

(a)

(b)

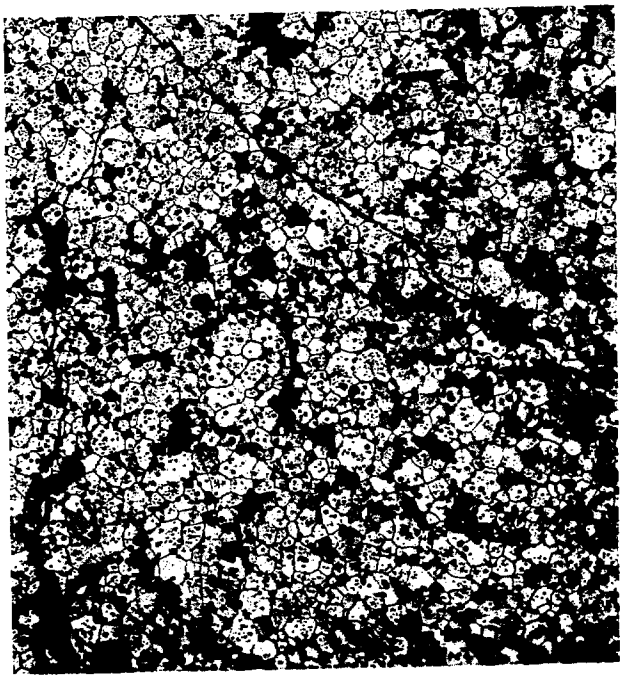

(c)

Fig. 40. Ceramographic specimen obtained from the central portion of fuel pellet SR-106. (a) Macrograph, as-polished, 10X; (b) as-polished, 100X; and (c) etched, 100X.

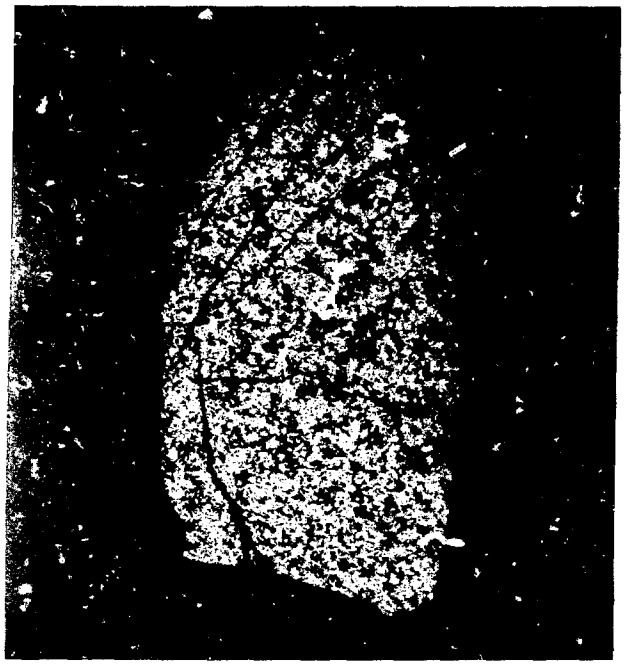

(a)

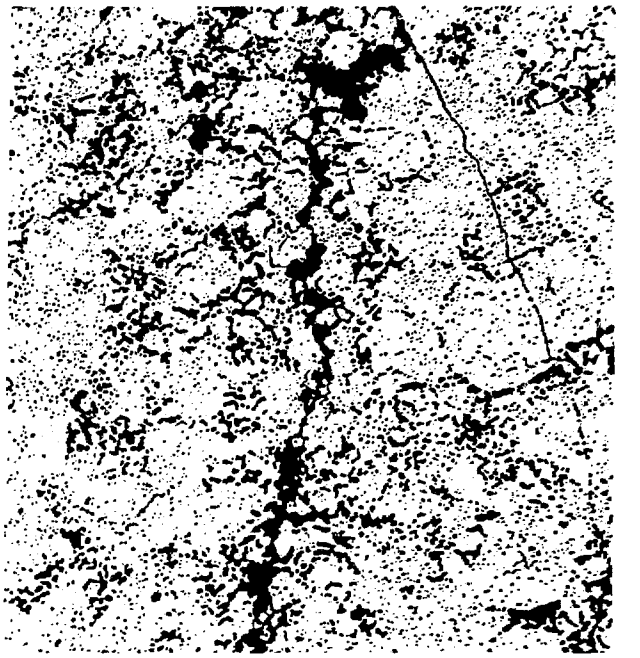

(b)

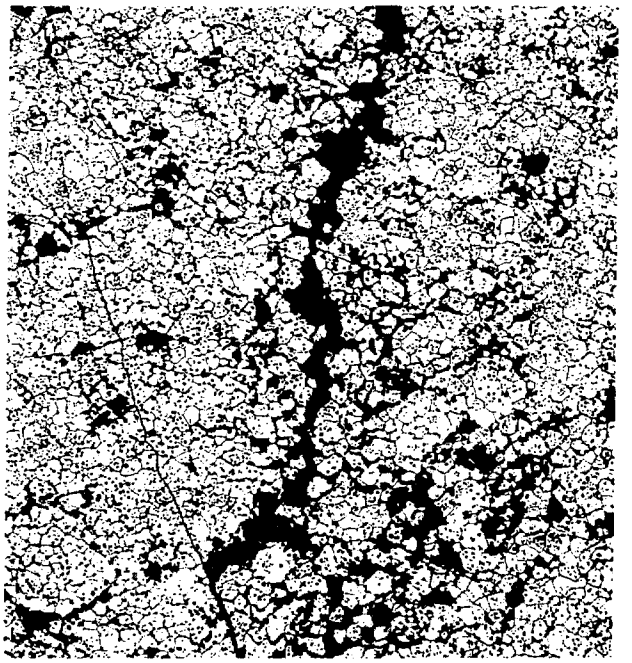

(c)

Fig. 41. Ceramographic specimen obtained from the external portion of SR-106. (a) Macrograph, as-polished, 10X; (b) micrograph, as-polished, 100X; and (c) etched, 100X.

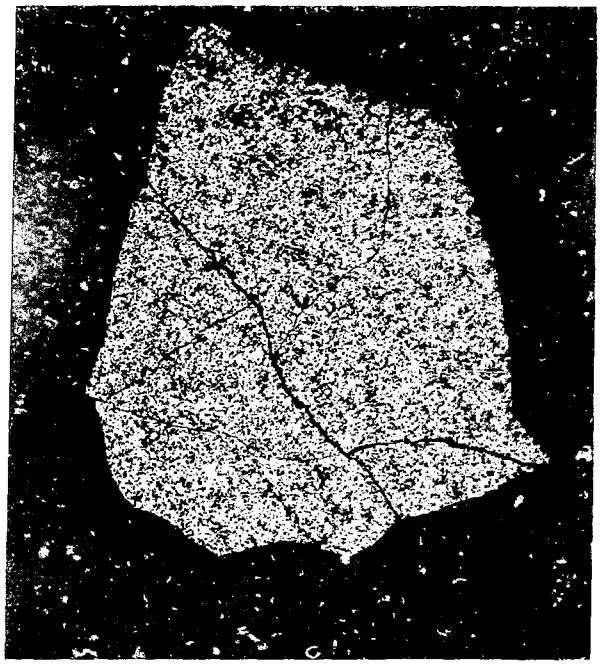

(a)

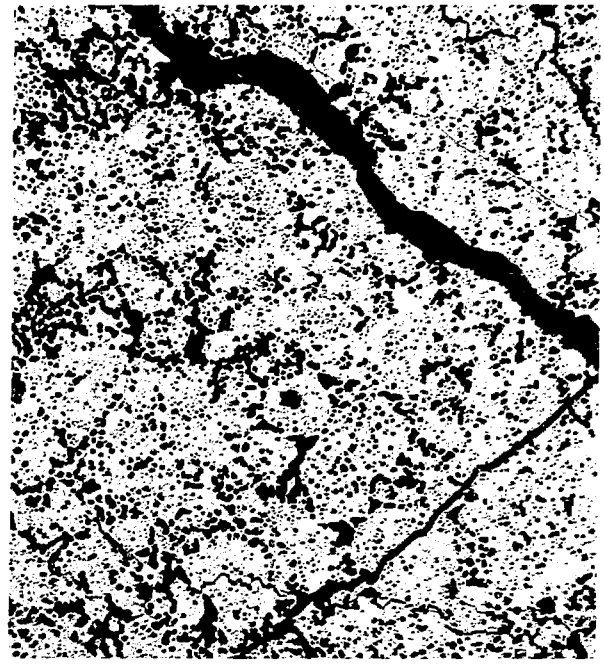

(b)

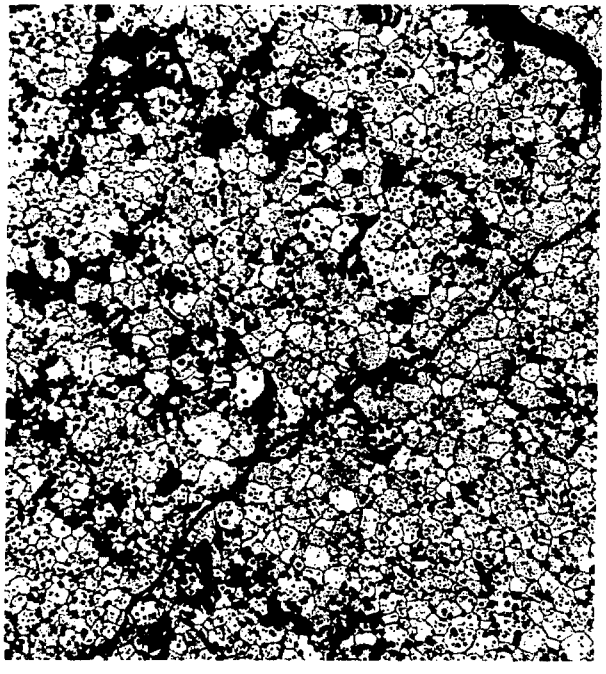

(c)

Fig. 42. Ceramographic specimen obtained from the central portion of fuel pellet SR-107. (a) Macrograph, as-polished, 10X; (b) micrograph, as-polished, 100X; and (c) etched, 100X.

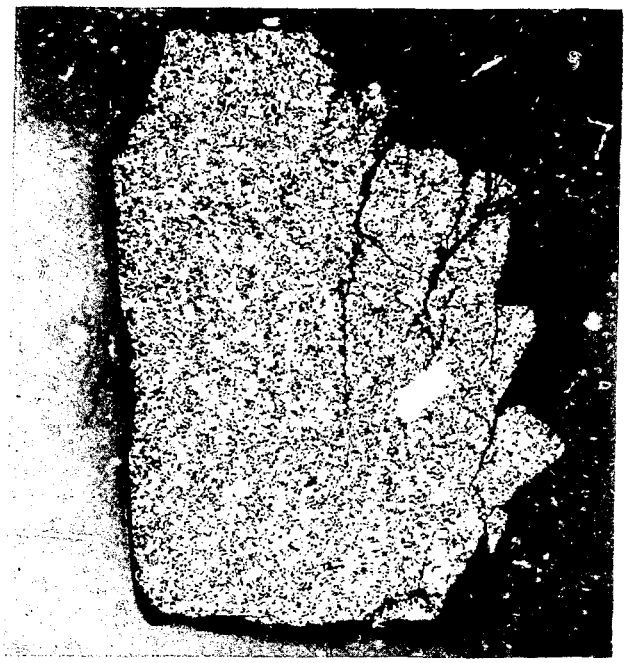

(a)

(b)

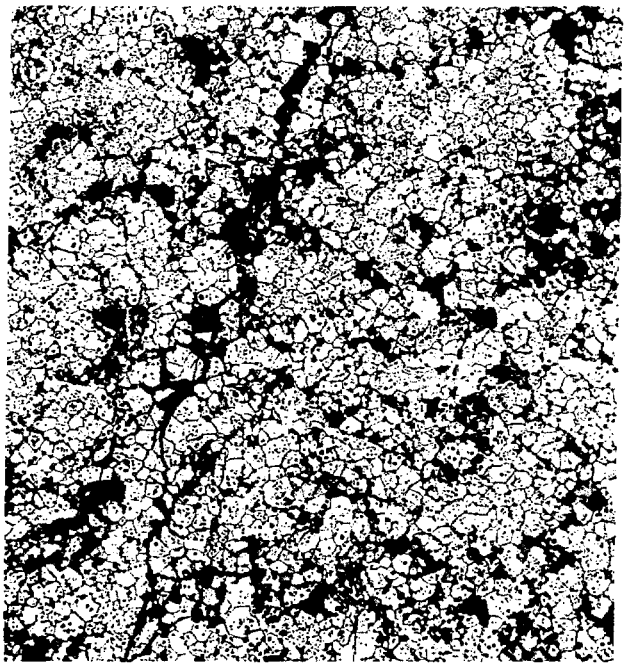

(c)

Fig. 43. Ceramographic specimen obtained from the external portion of SR-107. (a) Macrograph, as-polished, 10X; (b) micrograph, as-polished, 100X; and (c) etched, 100X.

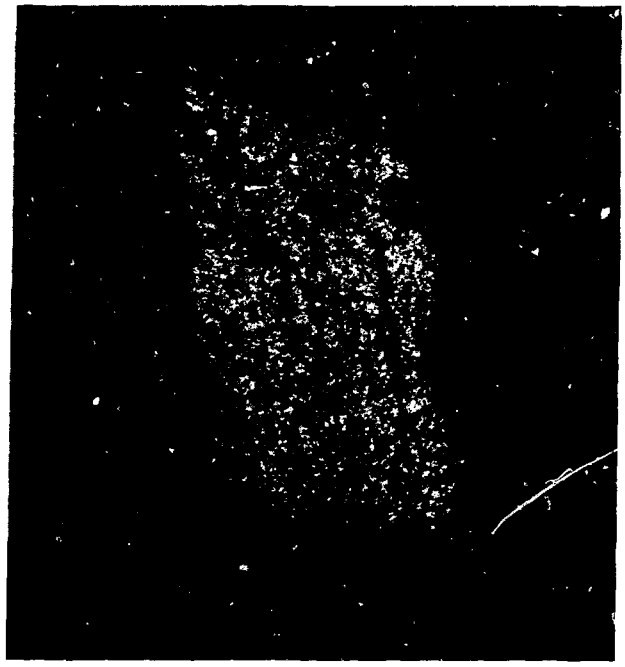

(a)

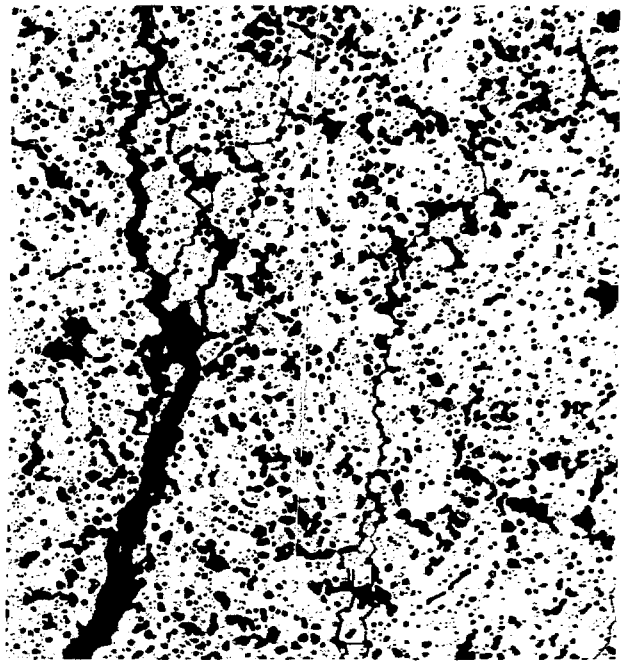

(b)

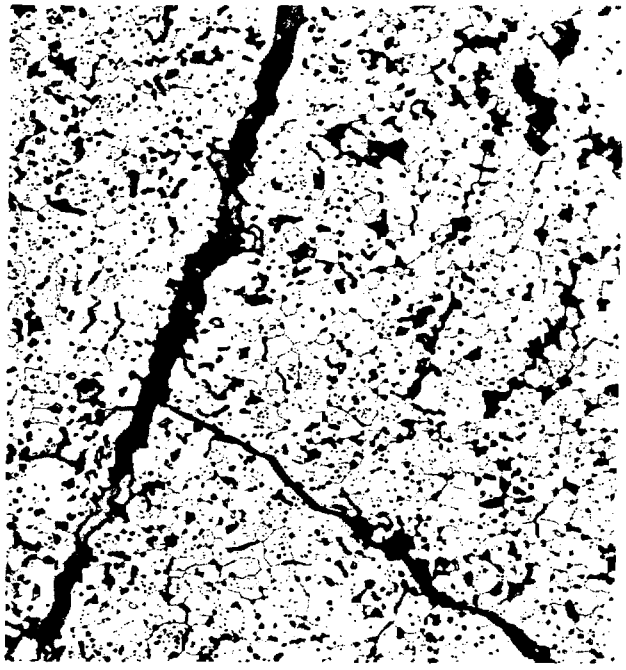

(c)

Fig. 44. Ceramographic specimen obtained from the central portion of fuel pellet SR-110. (a) Macrograph, as-polished, 10X; (b) micrograph, as-polished, 100X; and (c) etched, 100X.

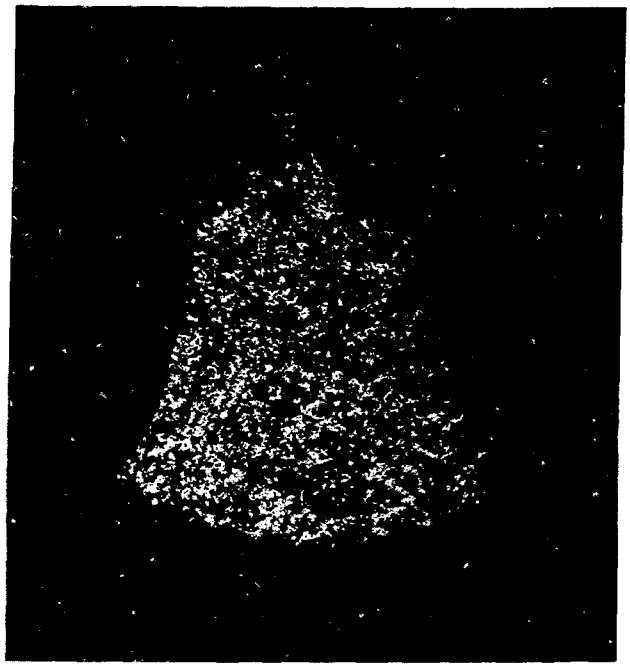

(a)

(b)

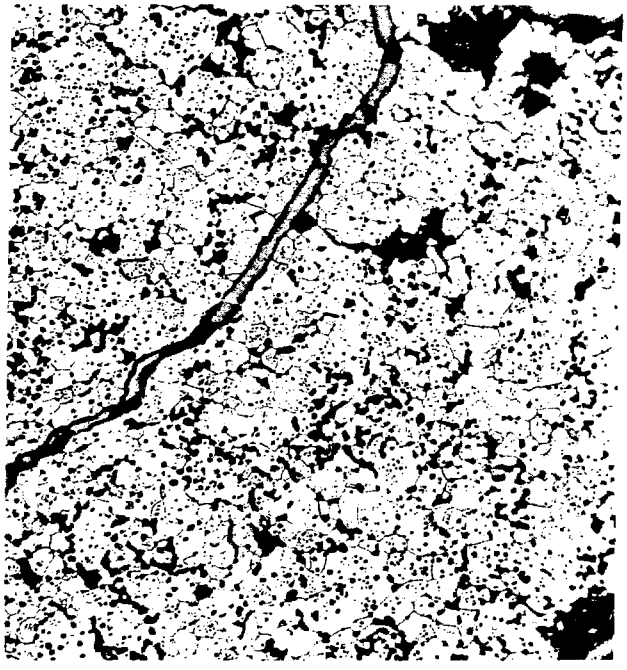

(c)

Fig. 45. Ceramographic specimen obtained from the external portion of SR-110. (a) Macrograph, as-polished, 10X; (b) micrograph, as-polished, 100X; and (c) etched, 100X.

☆U.S. GOVERNMENT PRINTING OFFICE: 1984-0-776-026/4114